

Role of cobalt oxide nanoparticles in CuTl-based superconductor



by

Muhammad Zareef Khan

267/FBAS/MS-PHY/S14

**Submitted in partial fulfillment of the
Requirement of the MS (Physics) degree**

Supervisor

Dr. Kashif Nadeem

Assistant Professor

Department of Physics

Faculty of Basic and Applied Sciences

International Islamic University,

Islamabad, Pakistan

(2016)





TH-16691

Wm

Accession No

MIS
670.5
KHR

1. Neurostructure
2. Neurochemistry

Role of cobalt oxide nanoparticles in CuTl-based superconductor

by:

Muhammad Zareef Khan
(267-FBAS/MSPHY/S14)

This Thesis submitted to Department of Physics International Islamic University,
Islamabad for the award of degree of MS Physics.



Chairman Department of Physics
International Islamic University, Islamabad.

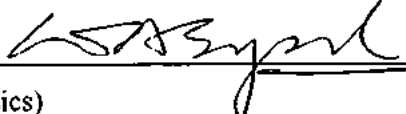


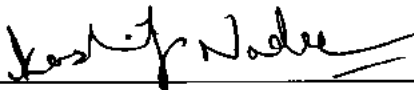
Dean Faculty of Basic and Applied Sciences
International Islamic University, Islamabad.

Final Approval

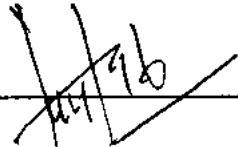
It is certified that the work presented in this thesis entitled "**Role of cobalt oxide nanoparticles in CuTi-based superconductor**" by **Muhammad Zareef Khan** Registration No. 267-FBAS/MSPHY/S14 fulfills the requirement for the award of degree of MS Physics from Department of Physics, International Islamic University, Islamabad, Pakistan.

Viva Voce Committee

Chairman 
(Department of Physics)

Supervisor 

External Examiner 

Internal Examiner 

بِسْمِ اللَّهِ الرَّحْمَنِ الرَّحِيمِ

First of All Thanks To Allah Almighty
This report is dedicated to my beloved parents and my great teachers.

DECLARATION

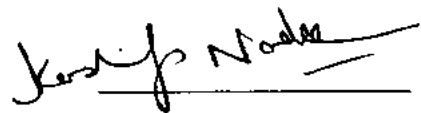
I am Muhammad Zareef Khan student of MS in Physics (session 2014-2016), hereby declare that the matter printed in the research project entitled “**Role of cobalt oxide nanoparticles in CuTi-based superconductor**” is my own work and has not been published or submitted as research work or project/thesis in any form in any other university or institute in Pakistan or abroad.


Muhammad Zareef Khan
267-FBAS-MS/Phy-S14

Dated: 24-02-16

FORWARDING SHEET BY RESEARCH SUPERVISOR

The research project entitled "Role of cobalt oxide nanoparticles in CuTI-based superconductor" submitted by **Muhammad Zareef Khan** in partial fulfillment of MS (Physics) has been completed under my guidance and supervision. I am satisfied with the quality of student's research work and allow them to submit this thesis for further process to complete their MS degree from Department of Physics, as per IIUI rules and regulations.



Dr. Kashif Nadeem

(Supervisor)

Assistant Professor

Department of Physics,

International Islamic University,

Date: 24-02-16

ACKNOWLEDGMENT

First, I owe my deepest gratitude to **Allah Almighty** for all of his countless blessings. I offer my humblest words of thanks to his most noble messenger **Prophet Muhammad ﷺ** who is forever a torch of guidance and knowledge for all humanity. By virtue of his blessings today, I am able to carry out our research work and present it.

I would like to express our special thanks of gratitude to my teacher, supervisor **Dr. Kashif Nadeem**, who gave me this golden opportunity to work on this project, who guided and supported me during my research work. Moreover, under his supervision from the preliminary to the concluding level enabled me to understand the field. His wide and deep knowledge have been a great value for me. May Allah Almighty bless him in every part of his life.

I would also like to express my heartiest thanks to **Dr. Yaqoob (NCP)**, who helped me for my samples characterizations. I will express my heartiest thanks to my seniors **Abdul Jabbar** and **Ghulam Hussain** for being very supportive and co-operative throughout my research work.

At last, but not the least, I am forever indebted to my parents and family members mother, father, brothers and sisters for their prayers, continuous support, love, understanding, endless patience, encouragement and their all possible help throughout the time of research work, without their help and understanding this work could not have been completed.

Table of Contents

Introduction	1
1.1 Superconductivity	1
1.2 Characteristics of Superconductors	3
1.2.1 Zero Resistivity	3
1.2.2 Zero Magnetic Induction	4
1.3 Superconductor experimental effects	5
1.3.1 Josephson Effect	6
1.3.2 Stationary Josephson Effect	6
1.3.3 Non-stationary Josephson Effect	6
1.4 The Meissner Effect	6
1.5 Ginzburg-Landau (GL) Theory	8
1.6 BCS Theory	9
1.6.1 Predictions of BCS theory	9
1.6.1.1 Critical field variation with temperature	10
1.6.1.2 Isotope Effect	10
1.6.1.3 Energy Gap	10
1.6.1.4 Magnetic Flux Quantization	11
1.6.1.5 Coherence Length	11
1.7 Penetration Depth of a Magnetic Field in a Superconductor	12
1.8 Applications of Superconductors	13
1.9 Classification of Superconductors	14
1.9.1 Type I and Type II Superconductors	14
1.9.2 Critical Parameters of Superconductors	15
1.9.2.1 Critical Temperature (T_c)	15
1.9.2.2 Critical Field (H_c)	16
1.9.2.3 Critical Current (I_c)	16
1.10 High temperature Superconductors (HTSCs)	17
1.11 Copper Thallium Based HTSC	18
1.12 Vortices and Flux pinning	18
1.13 Nanoscience and Nanotechnology	19
1.13.1 Nanomaterials	20
1.13.2 Classification of Nanomaterials	20

References	22
Chapter 2	25
Literature Review	25
2.1 Literature review	25
References	30
Chapter 3	32
Synthesis and Characterization Techniques	32
3.1 Synthesis of Nanomaterials	32
3.1.1 Bottom up approach	32
3.1.2 Top down approach	32
3.2 Synthesis of Cobalt Oxide nanoparticles	33
3.3 Preparation of (Co₃O₄)_x/CuTi-based nano-superconductor composites	35
3.4 X-ray diffraction (XRD)	37
3.5 Scanning Electron Microscope	40
3.5.1 Secondary electrons	42
3.5.2 Backscattered electrons.....	42
3.5.3 Auger electrons	42
3.5 Fourier Transform Infrared (FTIR) spectroscopy	43
3.6 Resistivity measuring technique	44
References	47
Chapter 4	49
Results and Discussion	49
4.1 X-Ray Diffraction (XRD)	49
4.2.1 XRD Analysis of Co ₃ O ₄ Nanoparticles.....	49
4.2.2 XRD Analysis of Nano-Superconductor Composites	50
4.3 Scanning electron microscopy (SEM)	51
4.4 Fourier transforms infrared (FTIR) spectroscopy.....	53
4.5 Resistivity measurements	54
4.6 Activation energy	57
Conclusion	60
References	61

List of Figures

Fig. 1.1: Discovery of superconductivity at 4.2 K by Kammerlingh Onnes.....	1
Fig. 1.2: Magnetic lines of forces passing through the material at $T > T_c$ and $T < T_c$	2
Fig. 1.3: Year-wise discovery of superconductivity	3
Fig. 1.4: The dependence of resistivity of oxide superconductors on temperature	4
Fig. 1.5: The electronic behavior in normal and superconducting state	5
Fig. 1.6: The Meissner effect	8
Fig. 1.7: The electronic movements in one and two dimensional lattice,.....	9
Fig. 1.8: Penetration depth represents the surface current from the surface circles inside superconducting material	12
Fig. 1.9: Superconducting penetration depth in one dimension	13
Fig. 1.10: Type I and Type II superconductors.....	15
Fig. 1.11: The relationship between critical parameters showing by phase diagram	16
Fig. 1.12: Historical background of HTSC	17
Fig. 1.13: CuTl-based HTSC unit cell	18
Fig. 1.14: A magnet is holding superconductor in space in the direction of Lorentz force, also current and magnetic fields lines are shown	19
Fig. 1.15: Classification of nano-materials.....	21
Fig. 3.1: Top down method vs. bottom up method	33
Fig. 3.2: Flow chart for the synthesis of Co_3O_4 nanoparticles by sol-gel method.....	34
Fig. 3.3: Flow chart for the preparation of precursor material.....	36
Fig. 3.4: Flow chart for the synthesis of $(\text{Co}_3\text{O}_4)_x/\text{CuTl-1223}$ nanosuperconductor composites.....	36
Fig. 3.5: The lattice shape with angles and lengths	37
Fig. 3.6: A typical X-ray diffractometer	38
Fig. 3.7: Schematic diagram of Bragg's law.....	40
Fig. 3.8: Schematic diagram of SEM.....	41
Fig. 3.9: Emission of auger electrons and X-rays.....	42

Fig. 3.9: Emission of auger electrons and X-rays.....	42
Fig. 3.10: Michelson interferometer.....	44
Fig. 3.11: Four-probe method.....	45
Fig. 3.12: Demonstration of contracts of wire on specimen.....	46
Fig. 4.1: XRD spectra of (Co_3O_4) nanoparticles	50
Fig. 4.2: XRD spectra of $(\text{Co}_3\text{O}_4)_x/\text{CuTi-1223}$ with $x = 0, 0.25, 0.50, 1.0$ and 2.0 wt.%	51
Fig. 4.3: SEM images of bulk CuTi-1223 superconductor matrix at (a) $10 \mu\text{m}$ and (b) $5 \mu\text{m}$	52
Fig. 4.4: FTIR spectra of $(\text{Co}_3\text{O}_4)_x/\text{CuTi-1223}$ with $x = 0, 0.25, 0.50, 1.0$ and 2.0 wt.%.....	54
Fig. 4.5: RT measurements of $(\text{Co}_3\text{O}_4)_x/\text{CuTi-1223}$ composites with $x = 0, 0.25, 0.50, 1.0$ and 2.0 wt. %.....	55
Fig. 4.6: Variation of critical temperature with concentration of Co_3O_4 nanoparticles in $(\text{Co}_3\text{O}_4)_x/\text{CuTi-1223}$ nano-superconductor composites.....	56
Fig. 4.7: The resistivity at normal state vs. nanoparticles concentration plot of $(\text{Co}_3\text{O}_4)_x/\text{CuTi-1223}$ nano-superconductor composites.....	57
Fig. 4.8: Arrhenius plots of $(\text{Co}_3\text{O}_4)_x/\text{CuTi-1223}$ nano-superconductor composites with $x = 0, 0.25, 0.75, 1.0$ and 2.0 wt.%.....	58
Fig. 4.9: Variation of T_c and activation energy with concentration of (Co_3O_4) nanoparticles in $(\text{Co}_3\text{O}_4)_x/\text{CuTi-1223}$ nano-superconductor composites with $x = 0, 0.25, 0.75, 1.0$ and 2.0 wt.%.....	59

Abstract

The effects of cobalt oxide nanoparticles addition in CuTl-based high T_c superconductor properties have been studied. Cobalt oxide (Co_3O_4) nanoparticles and $(\text{Cu}_{0.5}\text{Tl}_{0.5})\text{Ba}_2\text{Ca}_2\text{Cu}_3\text{O}_{10.8}$ (CuTl-1223) superconducting material were prepared separately by using sol-gel and solid-state reaction method, respectively. These Co_3O_4 nanoparticles were mixed in appropriate ratio to CuTl-based matrix at the final stage of $(\text{Co}_3\text{O}_4)_x/\text{CuTl-1223}$; $x = 0, 0.25 \text{ wt.}\%, 0.5 \text{ wt.}\%, 1.0 \text{ wt.}\%$ and $2.0 \text{ wt.}\%$ nano-superconductor composites synthesis. The structure and physical properties of Co_3O_4 nanoparticles and $(\text{Co}_3\text{O}_4)_x/\text{CuTl-1223}$ nanoparticles-superconductor composites were investigated by using XRD, FTIR and PPMS techniques. There was no significant changes in lattice parameters and crystal structure of parent bulk CuTl-based superconductor were observed after the addition of Co_3O_4 nanoparticles, which provide an evidence that nanoparticles are settles at the grain boundaries. The presence of Co_3O_4 nanoparticles has reduced the voids and was improved the inter-grains connectivity. The dc-resistance vs. temperature measurements of these samples were measured by using PPMS. The zero resistivity critical temperature $T_{c(0)}$ of these composite samples were decreased by increasing the weight percentage addition of Co_3O_4 nanoparticles in the CuTl-1223 matrix, which can be attributed to improved inter-grains connectivity due to the magnetic nature of these nanoparticles. Also by increasing the nanoparticles concentration the normal states resistivity was found to increase. The decline in the activation energy due to increasing concentration of Co_2O_3 nanoparticles is attributed to nanoparticles magnetic agglomeration or inhomogeneous addition of the nanoparticles at higher concentration.

Chapter 1

Introduction

1.1 Superconductivity

The phenomenon of superconductivity is precisely zero electrical resistance and magnetic field ejection from certain materials below a characteristic temperature which is known as critical temperature denoted by (T_c). The electrical resistivity absolutely vanishes at critical temperature. The resistivity of superconducting material is zero ($\rho \sim 0$), under the condition $T < T_c$ and $\mu_0 H < \mu_0 H_c$, as discovered by Onnes as shown in Fig. 1.1 [1].

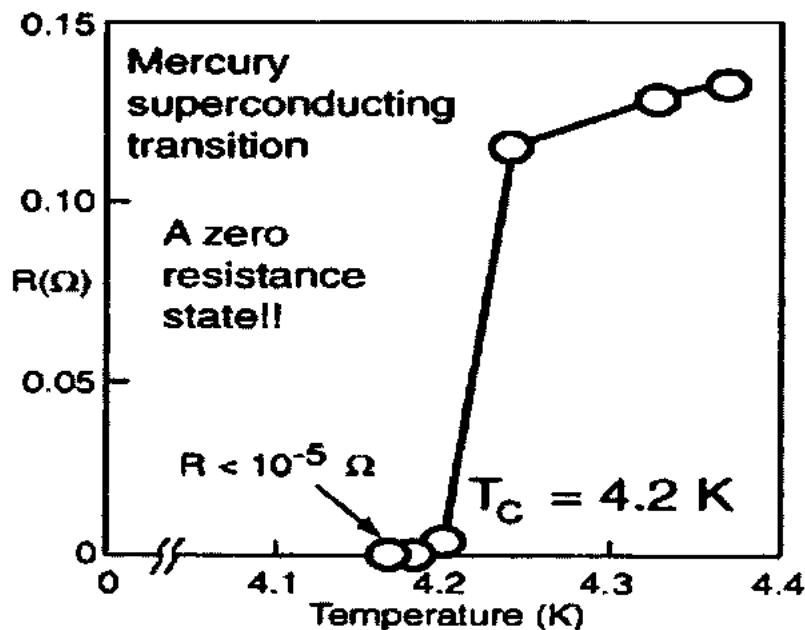


Fig. 0.1: Discovery of superconductivity at 4.2 K by Kammerlingh Onnes [2].

The magnetic field is completely expelled by the superconductor when its temperature is less than T_c . These forms conclude that at T_c , any other form of energy is dissipated. In 1911, a Dutch scientist named "Heike Kammerlingh Onnes" was the first scientist who discovered the superconductive material. In 1908, he was the first who liquefies helium and temperature reached as low as 1.7 K. In 1911, the superconductivity was observed in mercury (H_g) at liquid helium temperature below 4.2 K by "Heike Kammerlingh Onnes". After the discovery of superconductivity intensive research has been done on the superconducting materials and as a

result the most interesting properties of superconducting materials are discovered. So the discovery of superconductivity has brought a revolution in the field of solid state physics. Furthermore, emerging nanotechnology has created and revolutionized high performance materials and devices with amazing superconducting applications [3].

In 1935, two brothers F. and H. London found that below the critical temperature the magnetic field expelled from the superconducting material which carries superconducting current, it is due to the reduction of the electromagnetic free energy as shown in Fig. 1.2.

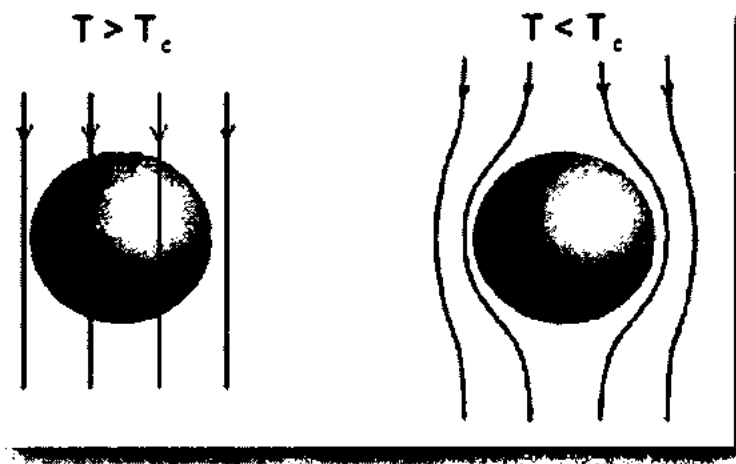


Fig. 1.2: Magnetic lines of forces passing through the material at $T > T_c$ and $T < T_c$ [4].

In 1957, J. Barden, L. Cooper and J. R. Schrieffer conferred a theory, termed as BCS theory in which the nature of superconductor was fully explained. The YBaCuO superconductor was also introduced with critical temperature at 90 K in 1987. In 1988 Bismuth Strontium Calcium Copper Oxide (BSCCO) also introduced superconductor with critical temperature at 110 K. The year-wise discovery of superconductivity is shown in Fig. 1.3 [5].

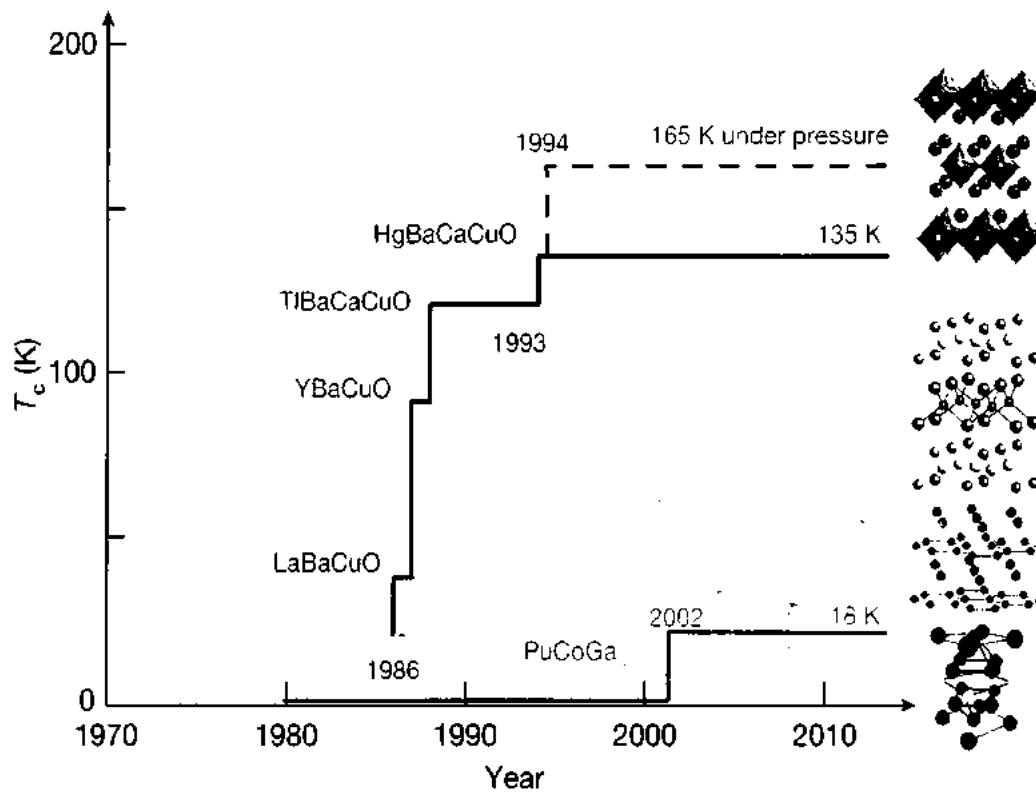


Fig. 1.3: Year-wise discovery of superconductivity [6].

1.2 Characteristics of Superconductors

There are many characteristics of superconductors which are very helpful in describing the phenomenon of superconductivity. The explanation of these parameters can help to understand the phenomenon of superconductivity. These parameters are discussed below.

1.2.1 Zero Resistivity

The resistance of the material vanishes below a specific limit of temperature is known as critical temperature (T_c). Certain experiments are performed to detect the resistivity of the materials. But when the current flows through the materials there will be some little resistance offered to flow of current that cannot be detected by introducing ammeter in the loop, also there will be decay of current due to resistance. The current flows through the superconductor are due to the electron pairs known as “Cooper pairs” [7]. The current has greater value than current density (J_c), which is passing through the conductor hence superconducting property, will be disappeared.

1.2.2 Zero Magnetic Induction

When magnetic flux is expelled from the interior of superconductor, the magnetic induction becomes zero then the materials are cooled below its T_c . The superconductivity disappears at a specific value of magnetic field is called critical magnetic field (H_c) [8]. When the charges move in the conductor the current is produced in the conductor. These moving charges collide with randomly moving atoms of the conductor which create obstacle to the flow of electrons. The lattice vibration or phonon and impurities may also offer opposition to the flow of free electrons that are moving through the conductor. The opposition offered to the flow of electrons is known as resistance. Due to increased temperature the resistance of the conductor also jumps to higher value. If temperature of the conductor reduces, the resistance also decreases below a certain critical temperature at which resistivity vanishes is shown in Fig. 1.4.

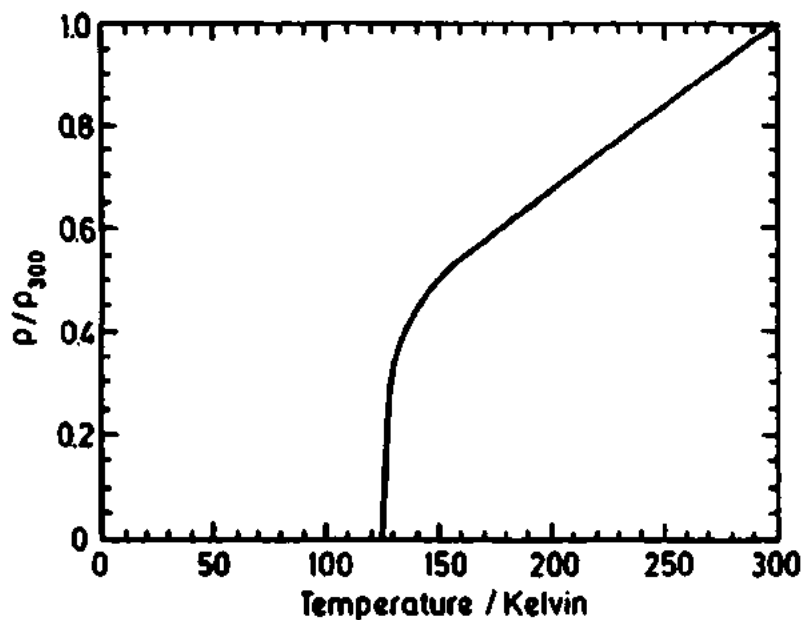


Fig. 1.4: The dependence of resistivity of oxide superconductors on temperature [9].

According to Coulomb's law in normal state there is repulsion between electrons. When the aluminum (Al) is cooled below its T_c , it changes electronic behavior from its normal state i.e. repulsive electron gas which consist of electrons in pair may also change into different types. Conduction electrons having spin and momentum couple with the electrons having opposite spin and momentum. The force for "Cooper pairs" is provided by the phonons which are indeed

lattice vibrations. Cooper pairs are formed by this attractive force. The Cooper pair's electrons are called as super-electrons. The normal state resistivity of conductor is caused by the impurities that further cause the scattering of conduction electrons. The electronic behavior is quite different in case of superconductors. It is not possible to undone the effect of cooper pairs ensembles the electron to take part in the superconducting state. A super current is established as a consequence flowing occurs without resistance. Single coherent motion is caused by the cooper pairs [10]. For individual repulsive electrons pair there is no scattering, mean there is no resistivity. Fig. 1.5 illustrates the electronic motion through the lattice.

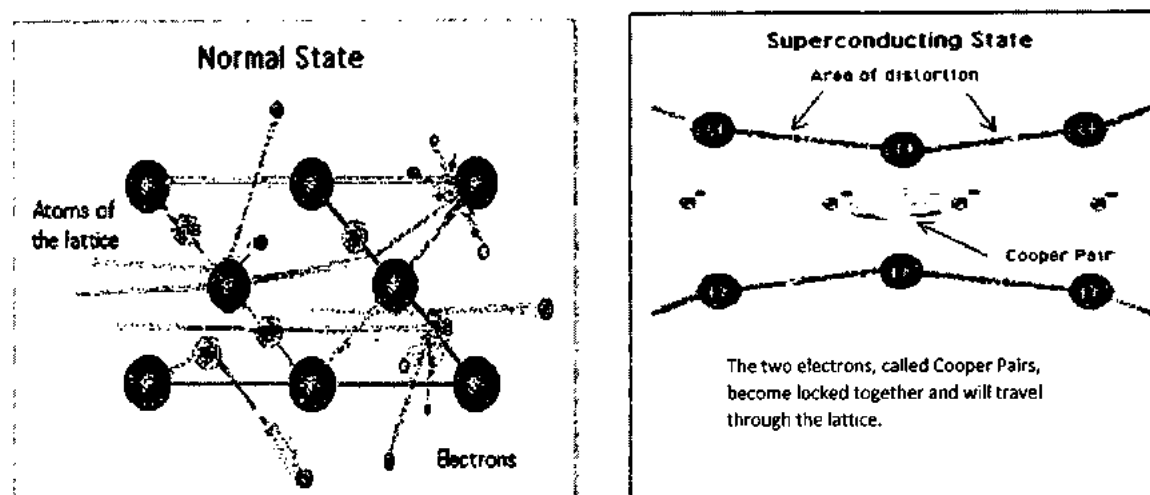


Fig. 1.5: The electronic behavior in normal and superconducting state [11].

The positive ionic core of the lattices is deformed when electrons pass through the lattices as well as their attraction deformed the lattices. This vibration of lattice is termed as phonon. Another electron approaches through positive ion core before retreating this vibration. The force to overcome the repulsion of electrons is provided by the phonons. The two electrons that are Cooper pairs locked together as a result they will travel through lattice [12].

1.3 Superconductor experimental effects

There are certain effects on the basis of which the superconducting phenomenon can be explained easily as discussed below.

1.3.1 Josephson Effect

Evidence of superconductivity was explained in 1962, on the basis of quantum mechanical expression which was given by the “Josephson’s Effect”. In this effect the tunnel junctions attract superconductor.

It has two types,

- i. Stationary Josephson effect
- ii. Non-stationary Josephson effect

1.3.2 Stationary Josephson Effect

Consider the DC effect in which we apply the current in tunnel junction. A very low current will pass through without any resistance in the junction. It is the result of electronic coherent behavior in superconducting state and the electron merge in a quantum body [13].

1.3.3 Non-stationary Josephson Effect

It is very astounding effect than DC effect. The value of DC current keeps on increasing across the links by applying a finite voltage to links. Beside the DC component ‘V’, voltage has ac component that is ‘ ω ’ (angular frequency).

$$\hbar\omega = 2eV \dots\dots\dots(1.1)$$

1.4 The Meissner Effect

This effect was observed in 1933 by W. Meissner and R. Ochsenfeld which shows the expulsion of magnetic field below certain transition temperature and critical magnetic field. This repulsion of magnetic field from the interior of superconductor is known as “Meissner effect”. The material shows zero magnetic fields inside it by the consideration of zero resistivity ($\rho \sim 0$), but it is an independent property [14].

Since,

$$B = \mu_0(H+M) \dots\dots\dots(1.2)$$

and

$$M = \chi H \dots\dots\dots(1.3)$$

Then it indicates that $\chi = -1$, it is the property of perfect diamagnetism.

A superconductor material must satisfy two conditions.

- 1- Having zero resistance.
- 2- It must eject weak magnetic field which indicates the Meissner effect.

If we consider a conductor having normal state then it will change its state from superconducting state to normal state and when it cools down below its critical temperature then it will change into superconducting state. By applying magnetic field across the conductor no field is passed as shown in Fig 1.6. The flux will be changed by the passage of field lines and current will be induced in it. The magnetic flux will be changed when the magnetic lines of forces passing through the specimen alters the flux induces current in the specimen. There is an interaction between applied magnetic field and internal magnetic field. Moreover, applied field is opposed by the internal magnetic field. There will be no field in the internal region of the specimen. This phenomenon cannot be explained from law of zero resistivity.

Using Maxwell's equation we can explain this phenomenon as given below

$$\nabla \times E = -j \frac{\partial B}{\partial t} \dots\dots\dots (1.4)$$

i.e. $E = 0$, for ideal conductor. It results

$$\frac{\partial B}{\partial t} = 0 \dots\dots\dots (1.5)$$

at all points.

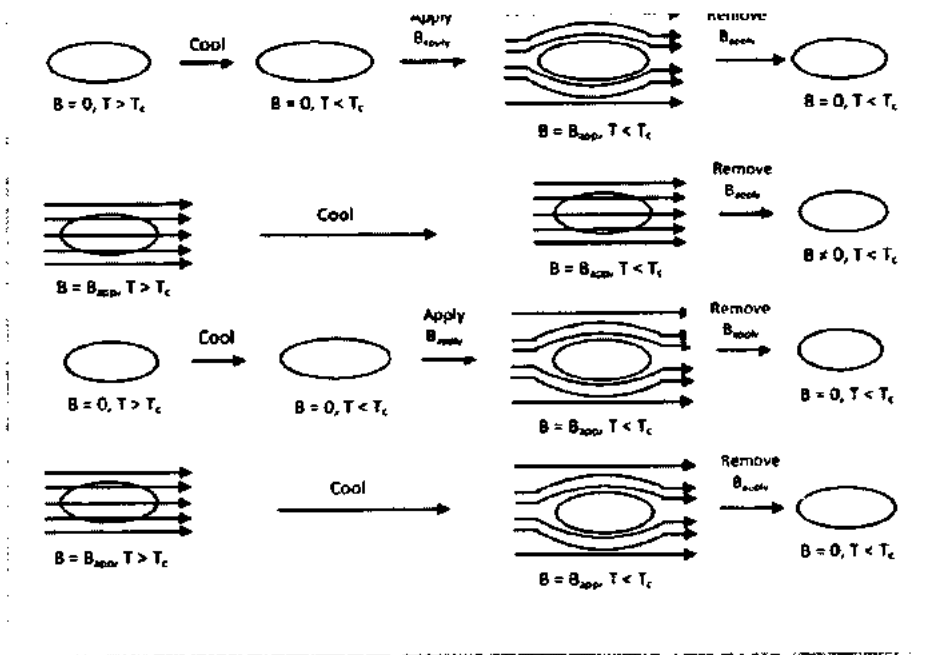


Fig. 1.6: The Meissner effect [15].

The characteristic of thermal equilibrium is Meissner effect but resistivity is non-equilibrium transport effect. The history of specimen has no effect on the final state. Superconductors can be defined as well as a system that reveals Meissner effect.

1.5 Ginzburg-Landau (GL) Theory

This theory was introduced by Ginzburg-Landau (GL) in order to find out the ordered parameter wave function Ψ for superconducting electrons having their local density $(ns) = |\Psi|^2$. In short, it leads to phase transition T_c for the carrier's density in terms of appropriate form of free energy (F). Ginzburg-Landau theory is associated to the superconductivity. The thermal fluctuation effect is introduced through the effect of this theory which is mostly considered negligible case of conservative low laws. However BCS theory establishes limit of T_c . From 1986 to onwards high temperature superconductors have been discovered extensively. In October 1993, highest T_c $\text{HgBa}_2\text{Ca}_2\text{Cu}_3\text{O}_{8-\delta}$ material was experimentally confirmed under pressure i.e $T_c \sim 150$ K [16]. There are some phenomenological features known but a complete fundamental theory is still unknown.

1.6 BCS Theory

In 1957, a theory presented by J. Bardeen, L.N. Cooper and J. S. Schrieffer named as BCS theory. This theory is successfully explained the certain phenomenon.

Two major aspects of this theory are,

- i. creation of “Cooper pair”
- ii. propagation of Cooper pairs without resistance

There is no resistance offered to electrons that are moving through the lattices in resonance with phonon. This interaction is described as electron phonons interaction by BCS theory [17]. The electrons propagate through the ion core. The BCS theory successfully explains the zero resistance phenomenon's in superconductors. The propagation of the electrons takes place through the ionic core. The lattices are distorted due to coulomb attraction between the ionic core and electrons are shown in Fig. 1.7.

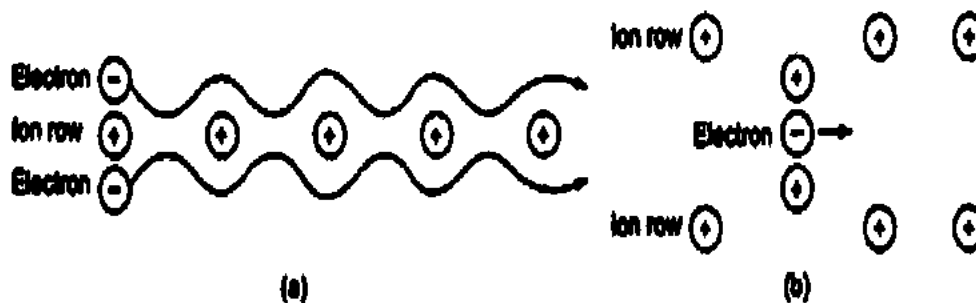


Fig. 1.7: The electronic movements in one and two dimensional lattice [18].

1.6.1 Predictions of BCS theory

This theory has given important predictions for the explanation of superconductivity which can explain the phenomenon of superconductivity easily.

- (a) Critical field variation with temperature,
- (b) Isotopic effect,
- (c) Existence of energy gap,
- (d) Magnetic flux quantization,

(e) Occurrence of coherence length.

1.6.1.1 Critical field variation with temperature

The prediction of critical magnetic field with temperature and also the isotopic effect phenomenon could be successfully explained by this theory. This theory also makes a prediction of existence of energy gap between excited state and ground state. This energy gap is required to break the Cooper pairs. There is more stability in the superconductors having large energy gap.

1.6.1.2 Isotope Effect

A large number of theories were proposed after the discovery of superconductivity but these are not enough to explain the motion of electrons in superconducting state. In 1950, Froehlich proposed that the mass of the isotopes varies with superconductor's transition temperature T_c . The phenomenon in which T_c increases by increasing atomic mass of that element is called isotopic effect.

The effect is illustrated by the following equation,

$$"M^\alpha T_c" = \text{Constant} \dots \dots \dots (1.6)$$

Where 'M' is the mass of isotopic superconductor and α is variation from material to material and its value is about 0.5. The interaction between electron and phonon effect has tremendous importance in superconducting state. The cause of zero resistance is zero interaction in between electron and phonon which is unique difference in the classical model of conduction [19].

1.6.1.3 Energy Gap

Energy gap is energy difference between ground state and superconducting state. The normal state electrons are above the Fermi level while the superconducting electrons are below Fermi surface. It is constant in case of superconductors and insulators.

It is maximum at 0 K i.e. absolute temperatures. At 0 K, the energy gap is given by

$$E_g(0) = 3.54 K T_c \dots \dots \dots (1.7)$$

We can say that at 0 K the pairing of electrons is complete. The pairing of electrons disappear when the temperature reaches to critical temperature, as a result energy gap becomes zero and superconducting phenomenon disappears [20]. There are many ground and excited states for superconducting electrons in the range from $T = 0$ to $T = T_c$. Electrons are in

state with complete phase coherence in such states. Below critical temperature phase coherence is vanished. When critical temperature is attained, pairs broke up which results in transition state i.e. superconducting material are converted in to normal conductor. The pairs broke up when the critical temperature is attained which results the transition of states i.e. the conversion of superconducting material into its normal state.

1.6.1.4 Magnetic Flux Quantization

In superconductors the “magnetic flux quantization” was predicted by BCS theory. In order to explain this phenomenon suppose a superconductor material in bulk form and having normal state i.e. $T > T_c$. Below its T_c , we reduce the temperature of specimen by applying the magnetic field H in the direction of axis of cylinder, normal to superconducting state is obtained by the sample. Some of the flux remains in the hole while the magnetic flux is pushed outwards from superconductor interior. The flux is caused by the super current that is induced at the interior of hole [21]. In 1961, magnetic flux was experimentally discovered in USA by B. Deaver and W. Fairbank and in Germany by R. Doll and M. Nabauer. The prediction of magnetic flux quantization was given by F. London according to which flux quantum must be (hc/e) and its value is twice which is greater than ‘ ϕ_0 ’ Where ‘ ϕ_0 ’ is the threshold value of magnetic flux which is given by,

$$\phi_0 = hc/2e \dots \dots \dots (1.8)$$

From above equation the numerical value of ‘ ϕ_0 ’ is $2.07 \times 10^{-7} \text{G-cm}^2$ This experiment also confirms that super current is due to pairs of electrons detected by the magnetic flux quantization.

1.6.1.5 Coherence Length

The characteristic property of superconductor is coherence length. The electron density changes over specific length and it cannot be change quickly in superconductors and after this state superconductivity disappear. This length is known as coherence length. This superconducting state depends upon energy gap, Fermi velocity of superconducting materials and charge carriers mean free path [22]. For example, when a material undergoes a transition from superconducting state to a normal state it consists of certain transition layers of specific thickness which is related to the coherence length.

It is given by equation,

$$\xi_o = \frac{\hbar v_f}{2E_g} \dots\dots\dots(1.9)$$

Where ' v_f ' represents the Fermi energy and ' E_g ' represents the energy gap of superconductor.

1.7 Penetration Depth of a Magnetic Field in a Superconductor

The depth over which there is exponential falls by 'e' times of the field strength from its original value is known as penetration depth. Fig. 1.8 shows the field on right side and area of superconductor on the left side of the boundary region which is shown by arrows. The black dots show the direction of flow of current outside the surface as shown in the Fig. 1.8. In superconducting material, there is a flow of current along the boundary region which screens the field to enter into the materials.

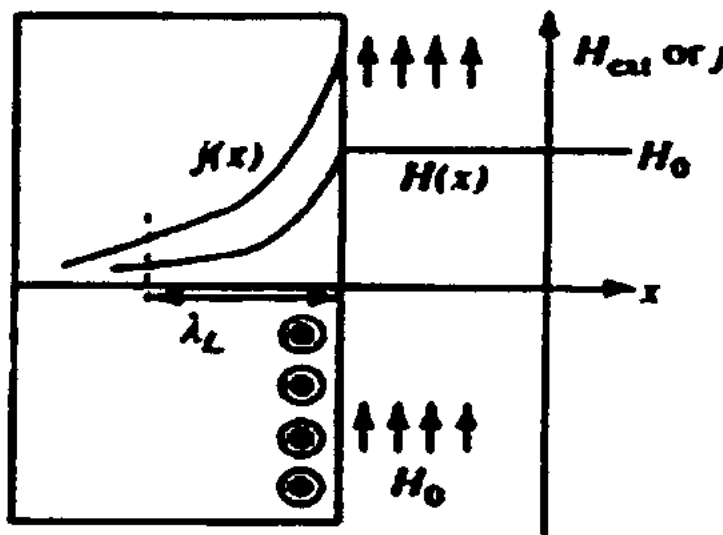


Fig. 1.8: Penetration depth represents the surface current from the surface circles inside superconducting material [23].

The current is flowing near the surface of the superconducting material and the material will be destroyed ultimately through the rise of the current density when the surface of the materials is narrowed. If the super current is uniformly distributed over the surface of the superconductors, the field will enter into the superconducting material up to same depth. The magnetic field strength (H_c) and current density (J_c) totally depend on

the depth of the material inside the surface. These two parameters gradually decrease when we proceed along the depth inside the material. The penetration depth is denoted by ' λ_L ' which is also called London penetration depth which depends upon the material nature and varies from material to materials as shown in Fig. 1.9 [24].

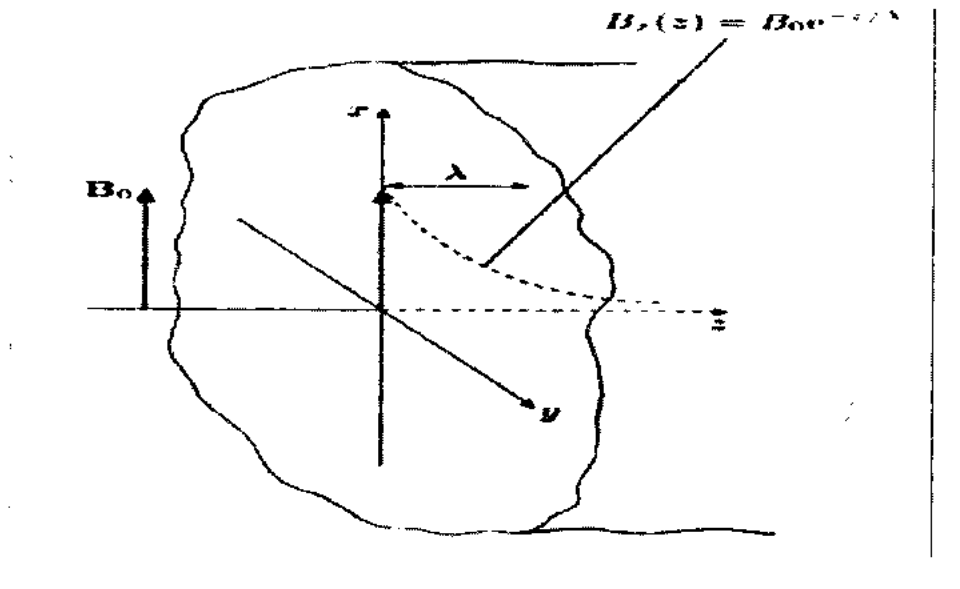


Fig. 1.9: Superconducting penetration depth in one dimension [25].

1.8 Applications of Superconductors

The enhancement in the technological application from scientific point of view and the discovery of high T_c superconducting materials are more important and play a vital role in the field of material science. Some of the important benefits from the discovery and technological application of superconductor are;

- ❖ Particle accelerator
- ❖ Magnetic resonance imaging (MRI)
- ❖ Microwave filters
- ❖ Superconducting quantum interference device (SQUID)
- ❖ Magnetic-levitation trains (Maglev)
- ❖ Quantum locking, etc.

1.9 Classification of Superconductors

Superconductors are the materials that have perfect diamagnetism and can be classified into two categories.

- ❖ Type I superconductors
- ❖ Type II superconductors

1.9.1 Type I and Type II Superconductors

It is observed that high magnetic field destroys the superconducting state and restore the normal state. Depending upon behavior of different materials with magnetic field, superconductor materials are divided into two categories i.e. type I superconductor and type II superconductor. In type I superconductors there is abrupt transition in magnetization verses applied magnetic field from perfect diamagnetic state to paramagnetic state. The critical field (B_c) for these types of superconductors is very low [26]. There are disadvantages to the use of these superconductors for practical applications due to low value of critical field hence they can't afford high currents.

On the other hand, the type II superconductors contain two critical fields H_{c1} and H_{c2} . The applied field penetrates partially into the material at H_{c1} and also the superconducting properties maintains at this field. At H_{c2} , the superconductivity completely vanishes which has much higher value. In type II superconductors there is no abrupt transition from perfect diamagnetic state to paramagnetic state [27]. There is a big advantage to use these types of superconductor for practical applications due to high value of critical field H_{c2} which is enable for making high superconducting wires of high field electromagnets is shown in Fig. 1.10.

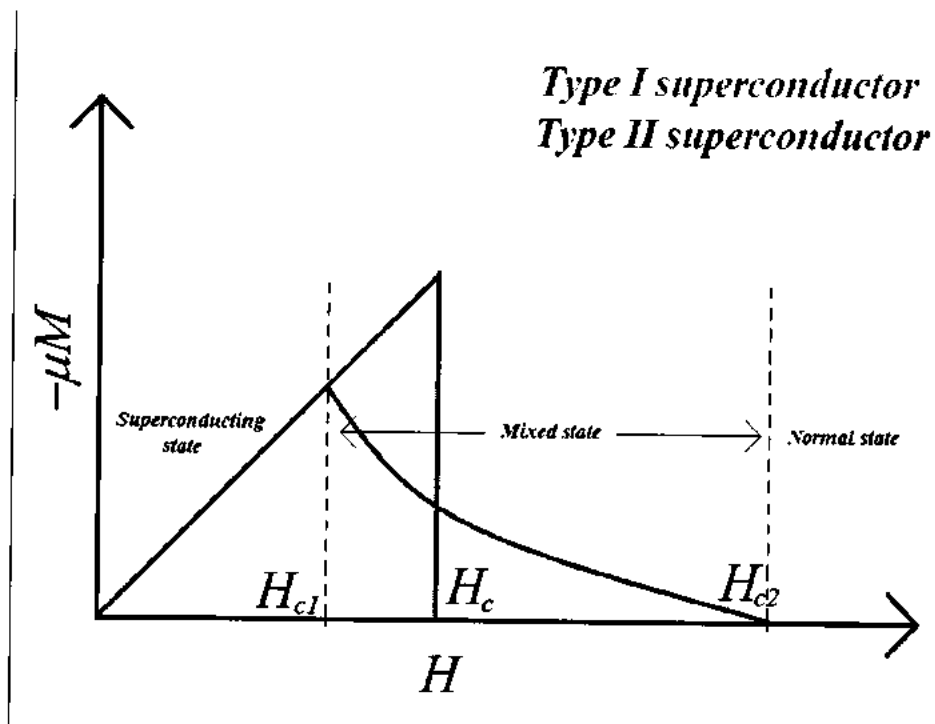


Fig. 1.10: Type I and type II superconductors [28].

1.9.2 Critical Parameters of Superconductors

There are certain parameters which are very crucial to describe the superconducting properties of a material.

- ❖ Critical Temperature (T_c)
- ❖ Critical Field (B_c)
- ❖ Critical Current density (J_c)

1.9.2.1 Critical Temperature (T_c)

The critical temperature is the temperature of the material at which its electrical resistance becomes zero and it denoted by T_c . At this temperature the material changes its state from normal to superconducting state. At this temperature the material changes its magnetic properties. At low temperature the superconducting phase transition is exhibited by certain materials and superconductivity occur below critical temperature T_c [29].

1.9.2.2 Critical Magnetic Field (H_c)

When a magnetic field is applied to a superconductor at a specific value of magnetic field superconductor shows transition from superconducting state to normal state. This magnetic field at which transition occurs is known as critical magnetic field denoted by ' H_c '. The value of critical magnetic field depends upon the nature of the material.

The relation between ' H_c ' and ' T_c ' is given by;

$$H_c(T) = H_0 \left[1 - \left(\frac{T}{T_c} \right) \right] \dots\dots\dots(1.10)$$

$H_c(0)$ maximum critical field occurring at 0 K and ' H_c ' is maximum critical field at ' T '.

The value of ' T_c ' value is lower for high value of critical field [30].

1.9.2.3 Critical Current (I_c)

The magnetic field generated by the current drives the material to normal state above the specific value of the current. If the value the magnetic field generated by the current exceeds the value critical magnetic field ' H_c ' then it derives the material from superconducting state to normal states. The corresponding value of current is known as critical current denoted by ' I_c ' [31]. The correlation between the critical parameter of superconductors is shown in the Fig. 1.11. The material is superconductor inside the curves which is the combination of these three factors and outside the curve it is in normal state.

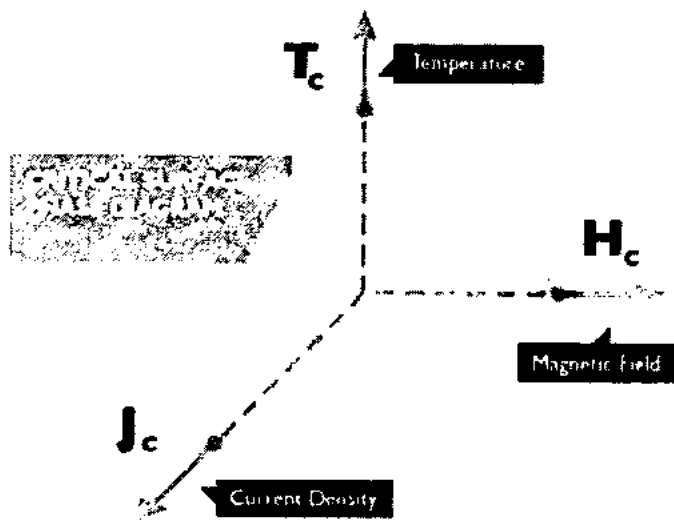


Fig. 1.11: The relationship between critical parameters showing by phase diagram [32]

1.10 High temperature Superconductors (HTSCs)

High temperature superconductors (HTSCs) are those materials that have temperature above 30 K. Scientists are trying to discover the superconductivity at room temperature which yet to be achieved. Discovery of HTSCs plays an vital role in the revolution of modern technology such as transmission storage and supercomputer technology. First HTSC was discovered in 1986 by Bednorz and Muller, and got Nobel Prize in 1987. The material was Yttrium-Barium-Copper-Oxide ($\text{YBa}_2\text{Cu}_3\text{O}_7$). From 1960 to 1980, 30 K was considered to be the highest theoretically possible transition temperature. IBM researcher's journals Karl Muller and Bednorz discovered first HTSC in 1986. The HTSC was used for cuprate superconductors such as Bismuth Strontium Calcium Copper Oxide (BSCCO) and Yttrium Barium Copper Oxide (YBCO). These materials show superconductivity at high temperature i.e. they are superconductive at the temperature of liquid nitrogen. The two series of cuprate compound having transition temperature in between 60 K and 120 K are Bi-Sr-Ca-Cu-O and Tl-Ba-Ca-Cu-O. They have typically orthorhombic or tetragonal structures [33, 34].

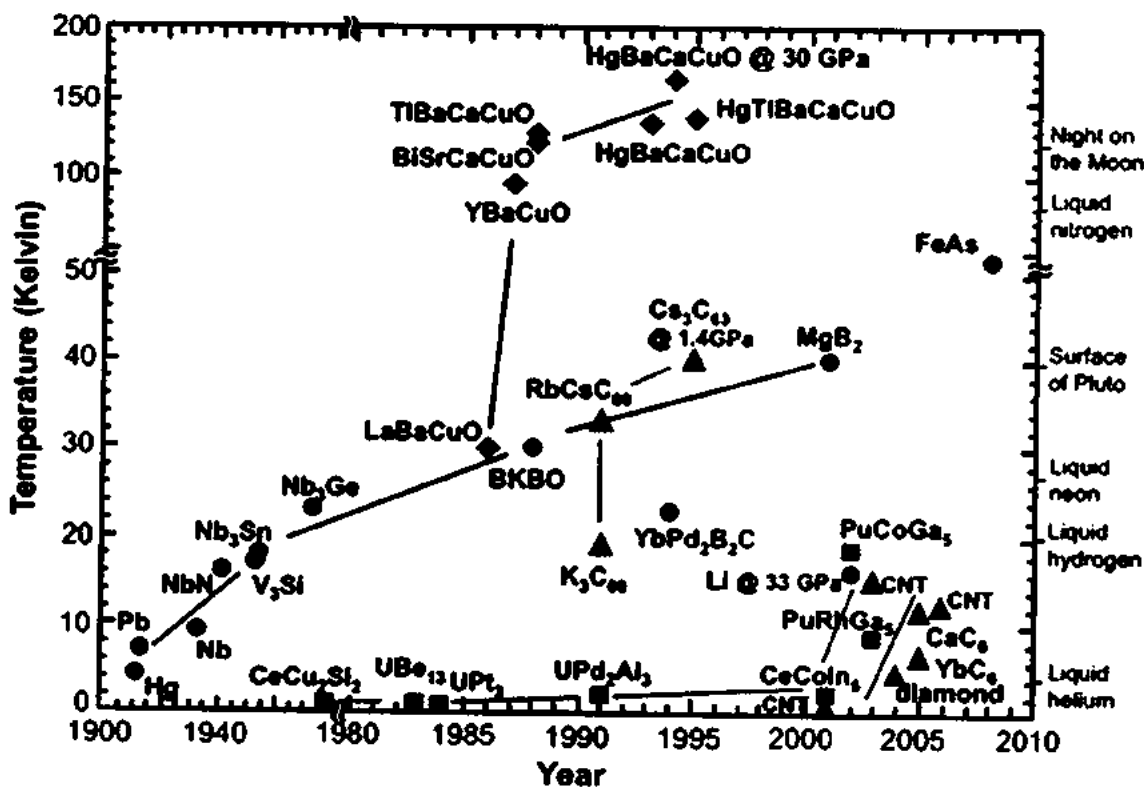


Fig. 1.12: Historical background of HTSC [35].

1.11 Copper Thallium Based HTSC

There are two Cu-based HTSCs families having higher superconducting parameters but their synthesis at ambient pressure is not possible. By adding Tl at Cu sites in Cu-12(n-1)n; (n = 2,3,4) superconductor a new sub family can be prepared easily by single step method at ambient conditions [36]. This subfamily having tetragonal structure with space group of P4/mmm and lattice constants around $a = 4.37 \text{ \AA}$ $b = 4.37 \text{ \AA}$ and $c = 14.82 \text{ \AA}$ has unit cell which is shown in Fig 1.13.

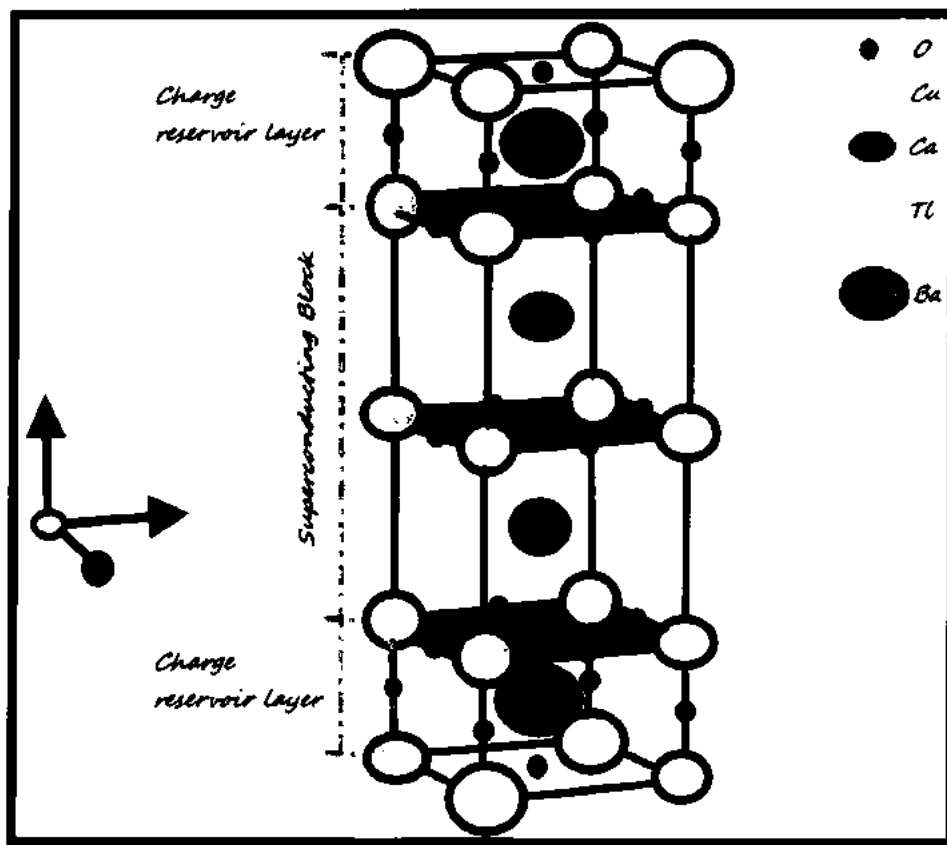


Fig. 1.13: CuTl-based HTSC unit cell [37].

1.12 Vortices and Flux pinning

The pinning of superconductor in space above the magnet is known as flux pinning phenomenon. In type II superconductor the vortices are created by the examination of superconductors. The magnetic field gradually passes through the superconductor during the vortices state. The flux pinning is made possible by the penetration of magnetic field due to which there will be partial penetration of the magnetic field over superconductors. The non-

homogenous type II superconductor contains defect between H_{c1} and H_{c2} and vortices are connected by defects. The vortices interact with the different types of defects and often these interactions show attractiveness nature. Finally the vortices are connected with these types of defects. Due to these prominent features the superconductor is able to carry some current and also there is no energy dissipation in superconductor. This process is carried on up to time when the pinning force becomes larger than the Lorentz force. There will be some loss of energy when the flux is generated in the direction of Lorentz force [38]. In type II superconductor due to the defects the flux pinning can be illustrated in the existence of magnetic field. The illustration of type II superconductors in the existence of magnetic field and vortices pinning due to defects are shown in Fig. 1.14.

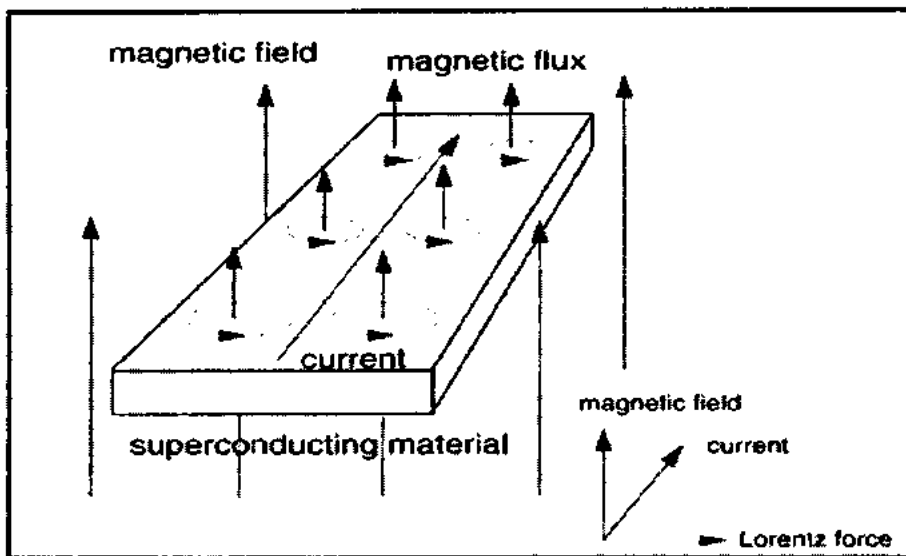


Fig. 1.14: A magnet is holding superconductor in space in the direction of Lorentz force, also current and magnetic fields lines are shown [39].

1.13 Nanoscience and Nanotechnology

The nano is Greek word which means 'dwarf'. It is the study of the materials at nanoscale. One nanometer is very small and it is about one billionth part of meter or 10^{-9} m. Nanoscale based materials exist in between 1 and 100 nm. Nanotechnology has a great impact in application of our present technology. It is the field that plays a vital role in the revolution of many aspects of technologies and it has a great impact in different commercial and industrial fields of life. So nanotechnology is basically the engineering of the materials at nano-scale level.

The fabrication and structure of the materials that's have dimension in the range of 100 nm are discussed in this field. The field of nanotechnology is progressing rapidly day by day but there is no prediction to the future of this technology. Nanotechnology is very efficient technology because great accuracy is obtained through the reduction in the size of the devices and materials. Also the future prospectus of human depends upon new discoveries and technology which makes our environment and life better [40].

1.13.1 Nanomaterials

Nanomaterials are small sized materials which can't be seen through eyes. At least one dimension of the nanomaterial is less than 1 μm . These materials posses both type of structure i.e crystalline or amorphous. One nanometer is so small and it is equal to one millionth of a millimeter which is about 100,000 times smaller than the diameter of human hair. Nanomaterial exhibits unique optical, electrical, magnetic and many other properties at nanoscale. The nano-scale material shows different and unique properties from the materials at bulk. The reason for the difference in the properties of materials at nanoscale is due to the increase in the surface area of and new quantum effects. The materials at nanoscale have high Quantum effects are also helpful in determining the surface to volume ratio than the bulk which results into great chemical reactions and also the strength of the materials increases properties of nanomaterials at nano-scale can be determined easily than the bulk which leads these materials into a great chemical reactions and also strengthen the materials. The materials at nano level possess high quantum effect and also nanomaterials occur naturally but for our particular interest they are engineered for many important products. Examples of nanomaterials are carbon nanotubes fullerene etc [41].

1.13.2 Classification of Nanomaterials

The materials can be classified in to two types on the basis of dimensions.

- ❖ Zero dimensional
- ❖ One dimensional
- ❖ Two dimensional

In zero dimensional (0D) all the dimensions are in the range of 100nm and all the dimensions are measured in nanoscale. The 0D nanomaterials could have amorphous or crystalline structure. Examples of zero dimensional materials include nanoclusters and spheres [42]. In one dimensional (1D) nanomaterials, only one dimension is measured outside the

nanoscale. They could have a crystalline or amorphous structure. Examples of 1D nanomaterial are nanofibers, nanowires and nanorods. In two dimensional (2D) nanomaterials, the two dimensions of material are outside the nanoscale. They are made up of various chemical compositions. Examples of 2D materials are nanofilms, nanocoating etc. In three dimensional 3D nanomaterials, no dimensions are in nanoscale, all the dimensions of the material are above than 100 nm. These materials are also known as bulk nano-materials. These materials are characterized as having 3 arbitrary dimensions above 100 nm which are shown in Fig. 1.15, where a, b, c and d shows different dimension of nanomaterials i.e. 0D, 1D, 2D and 3D respectively [43].

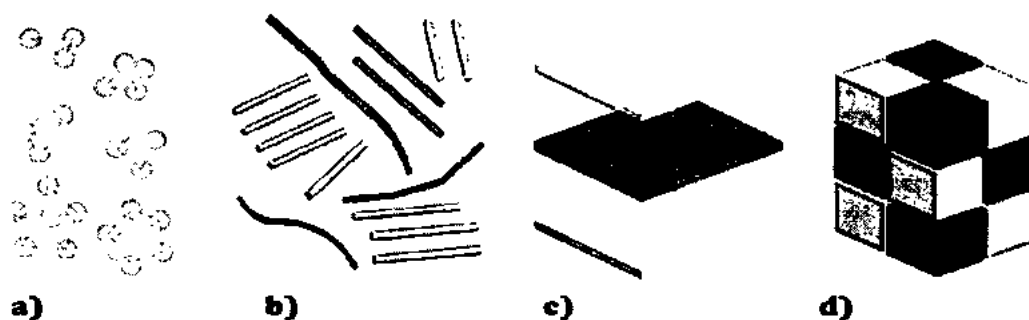


Fig. 1.15: Classification of nanomaterials [44].

References

1. M. Tinkham, "Introduction to Superconductivity", 2nd Ed. Dover Publications (2004).
2. <http://philschatz.com/physics-book/contents/m42709.html>
3. A.C. Rose Innes and E. H. Rhoderick, "Introduction to Superconductivity" Pergamon Press, Oxford UK (1969).
4. https://en.wikipedia.org/wiki/Meissner_effect
5. J. Bardeen, L. N. Cooper, and J. R. Schrieffer, "Theory of superconductivity" Phys. Rev. **108**, 1175 (1957).
6. http://www.nature.com/nature/journal/v518/n7538/fig_tab/nature14165_F1.html
7. H. Ibach, H. Lüth, "Solid State Physics: An Introduction to Principles of Materials Science", 2nd Edition, Springer (1995).
8. J. P. Srivastava, "Elements of Solid State Physics" PHI Learning Pvt. Ltd. (2011).
9. S. Larsson, "Chemical Physics: Electrons and Excitations" CRC Press (2012).
10. V. V. Schmidt, P. Muller, and A. V. Ostinov, "The Physics of Superconductors: introduction to Fundamentals and Application" Springer-Verlag, Berlin (1997).
11. <http://nptel.ac.in/courses/113104005/89>
12. S. O Pillai, "Applied Physics", New. Age. International (2006).
13. A. Parinov, "Microstructure and Properties of High-Temperature Superconductors", 2nd Edition, Springer Science & Business Media (2013).
14. W. Meissner and R. Ochsenfeld, "Landmark Experiments in twentieth century physics" Naturwissenschaften **21**, 787 (1933).
15. <http://users-phys.au.dk/philip/pictures/physicsfigures/physicsfigures.html>
16. M. S. Vijaya, G. Rangarajan, "Material science" McGraw-Hill (2003).
17. G. Aruldas, P. Rajagopal, "Modern Physics" PHI Learning Pvt. Ltd. (2005).
18. <http://chemiris.chem.binghamton.edu/chem445/HighTc/HighTc.htm>
19. R. P. Huebener, Conductors, Semiconductors, Superconductors: "An Introduction to Solid State Physics" Springer (2014).
20. E. O'Reilly, "Quantum Theory of Solids" CRC Press (2003).
21. X. F. Pang, Y. P. Feng, "Quantum Mechanics in Nonlinear Systems" World Scientific (2005).
22. N. Mehta, "Textbook of Engineering Physics" Volume II, PHI Learning Pvt. Ltd. (2009).

22. N. Mehta, "Textbook of Engineering Physics" Volume II, PHI Learning Pvt. Ltd. (2009).
23. https://en.wikipedia.org/wiki/London_penetration_depth
24. Joshi, "Engineering Physics" McGraw-Hill Education (2010).
25. <http://cmms.triumf.ca/theses/Sonier/MSc/node8.html>
26. Michael Tinkham, "Introduction to Superconductivity" 2nd Ed. Dover Publications (2004).
27. A.C Rose Innes, and E. H. Rhoderick, "Introduction to Superconductivity" Pergamon Press, Oxford UK (1969).
28. https://commons.wikimedia.org/wiki/File:Magnetisation_and_superconductors.png
29. G. B. S. Narang, and R. C. Gupta, "Materials Science" 7th Ed. Khanna, New Delhi (1993).
30. V.V. Schmidt, P. Muller, and A. V. Ostinov, "The Physics of Superconductors: Introduction to Fundamentals and Application" Springer-Verlag, Berlin (1997).
31. C. P. Poole, Jr., H. A. Farach, and R. J. Creswick, "Superconductivity" 3rd Ed. Elsevier, Netherlands (2014).
32. <http://www.htstria.com/superconductivity.html>
33. R. Abd-Shukor, F. A. Sc, "High Temperature Superconductors: Materials, Mechanism and Applications" Akademi Sains, Malaysia (2009).
34. A. Mourachkine, "High Temperature Superconductivity in Cuprates the Non-Linear Mechanism and Tunneling Measurements" Kluwar Academic, Brussels (2002).
35. <https://en.wikipedia.org/wiki/Superconductivity>
36. M. Hermann, and J. V. Yakhmi, "Thallium-Based high- Temperature Superconductors" Marcel Dekker, New York (1994).
37. <http://chemiris.chem.binghamton.edu/chem445/HighTc/HighTc.htm>
38. M. S. Vijaya, and G. Rangarajan, "Materials Science" Tata McGraw-Hill, New Delhi (2004).
39. <http://www.mn.uio.no/fysikk/english/research/groups/amks/superconductivity/mo/>
40. V. Pokropivny, R. Lohmus, I. Hussainova, A. Pokropivny, and S. Vlassov, "Introduction to nanomaterials and nanotechnology" Tartu University Press, Tartu (2007).
41. G. Mamails, L. O. G. Vogtlander, and A. Markopoulos, "Nanotechnology and nanostructured materials trends in carbon nanotubes" J. Precis. Eng, **28**, 16-30 (2002).

42. O. Manasreh, "Introduction to Nanomaterials and Devices" Wiley, New Jersey (2011).
43. Nouailhat, "An introduction to Nanoscience and Nanotechnology" Wiley, New Jersey (2010).
44. <https://nccr.itm.ac.in/2011.pdf>

Chapter 2

Literature Review

2.1 Literature review

Jabbar *et al.* [1] prepared $\{(Au)_x/CuTl-1223\}$ superconductor composites with $x=1.5\%$, 1.0% , and $0.5\text{ wt.}\%$ by two step method. They observed that gold (Au) nanoparticles did not effect on the superconducting properties of copper thallium matrix CuTl-1223. They used different techniques such as x-ray diffraction (XRD), morphology of the materials was examined by scanning electron microscopy (SEM), Fourier transform infrared (FTIR) spectroscopy, and resistivity (ρ) measurements. They analyzed that the CuTl-1223 crystal structure did not alter with the addition of Au nanoparticles. They observed that Au nanoparticles filled interstitial spaces, pores and improve the inter-grains connectivity. They also found that superconducting properties and volume fraction were also improved.

Cavdar *et al.* [2] prepared cuprates superconductors. They prepared composites to mix different materials such as $SrCO_3$, V_2O_5 , Bi_2O_3 , and $CaCO_3$ in the form of powder and heated for 90 minutes at $1150^\circ C$ and quenched between copper plates slowly. They determined the phase purity and crystalline of materials by using XRD technique. They measured the dielectric properties, tangent loss ($\tan\delta$) and AC conductivity (σ_{ac}) over the frequency range of 10 kHz to 10 MHz at 300 K. They also analyzed that dielectric properties are strongly frequency dependent and degree of heat. By the polarization effect negative capacitance (NC) phenomenon were also observed at low frequency range.

Cavdar *et al.* [3] prepared a high temperature superconductor family like i.e. $Tl_2Ba_2Ca_1Cu_2O_x$ and $Tl_2Ba_2Ca_2Cu_3O_x$. They characterized their samples by X-ray diffraction techniques. By the X-ray diffraction scan they observed that the materials contain Tl-2212 and Tl-2223 phase. They calculated unit cell parameter as Tl-2223 $a = b = c = 3.845\ 35.85$ also Tl-2212 for $a = b = c = 3.845\ 29.32$. They measured the dielectric properties, tangent loss and AC conductivity with the help of LCR meter. These parameters were calculated as the function of temperature 80-300 K and frequency range is (100 Hz-10 MHz). They observed the negative capacitance which strongly depends on the frequency and temperature. The dielectric properties, like real and imaginary part, tangent loss and Ac conductivity depend on the frequency range.

When the frequency increases the dielectric constant is also increase, at higher frequencies and temperature dielectric loss is approximately constant. At lower frequency and temperature the dielectric properties shows strong dispersion.

Jabbar *et al.* [4] prepared Al_2O_3 nanoparticles added CuTi-1223 superconductor by solid-state reaction method. They added the different concentration of Al_2O_3 nanoparticles with CuTi-1223. The $(\text{Al}_2\text{O}_3)_x/\text{CuTi-1223}$ composites were characterized by XRD, SEM, and resistivity measurement. They analyzed that the addition of Al_2O_3 nanoparticles did not affect the crystal structure of CuTi-1223 matrix. They observed that Al_2O_3 occupy the interstitials spaces and improve the inter-grains connectivity. By increasing the concentrations of Al_2O_3 the critical temperature (T_c), critical current density (J_c) and other superconducting properties were suppressed due to breaking of cooper pair mechanism. They also concluded that superconducting properties are non monotonic variation due to inhomogeneous distribution of Al_2O_3 at the grains boundaries.

Mohammed [5] investigated the effect of MgO on superconducting and dielectric properties of CuTi-1234 superconductor. The concentration of MgO changed from 0.0 to 1.0 wt. %. He characterized the composites by XRD and calculated the volume fraction of prepared compounds i.e. $x = 0.0, 0.2, 0.6,$ and 1.0% from room temperature. The critical room temperature was increased from 122 to 136 K as x increased from 0.0 to 0.8% and then for $x=1.0\%$ it decreased to 117 K. He also measured the dielectric properties of all prepared composites from 100 Hz to 4 MHz at 113 to 300 K. He concluded that for all values of x real part of dielectric constant (ϵ') has dependence upon both frequency and temperature. At lower temperature the value of tangent loss ($\tan\delta$) and imaginary part of dielectric constant show dispersion which shift toward low frequencies.

Jannah *et al.* [6] studied the effect of nano Co_3O_4 on the addition of Bi, Pb-2223 superconductors. They synthesized the composites by solid state reaction method. They did characterization by powder XRD, SEM and DC electrical resistivity by four probe methods. The crystal structure phase was confirmed by XRD. By adding the small amount of Co_3O_4 like 0.01wt.% superconducting properties were suppressed. The superconducting volume fraction was also reduced by increasing the contents. Due to magnetic nature of the composites, the normal states resistivity was also increased.

Awad *et al.* [7] investigated the bulk superconductor $(\text{MgO})_x/\text{Cu}_{0.25}\text{Tl}_{0.25}\text{Ba}_2\text{Ca}_3\text{Cu}_4\text{O}_{12-\delta}$ sample with $x=0, 0.2, 0.4, 0.6$ and 1 wt. %. MgO nanoparticles were synthesized through the method of single step solid state reaction. In a sample the nanoparticle containing size of 40nm to 60 nm were mixed simply and by the grinding process. Some peaks of other phases are observed including prevailing phase of $\text{Cu}_{0.25}\text{Tl}_{0.25}\text{-1234}$ superconductor sample through the XRD analysis. Scanning electron microscopy revealed the presence of nanoparticles between the grains. The micro hardness, connections between grain and J_c were observed as an increase due to MgO nanoparticles up to the concentration of x at 0.6 wt%.

Muhammad *et al.* [8] studied the sample CuTI-1223 superconductor, prepared by solid state reaction, doped with nano-particle of SnO_2 having from 0.1 wt. % to 1.0 wt. %. The tetragonal structure of sample CuTI-1223 is observed by XRD analysis with some peaks of secondary phases for instance BaCuO_2 and Cu-TI-1212. Peaks regarding to nano SnO or Sn based compound was found absent in the analysis of XRD. Also through XRD the volume fraction represents the limited percentage of CuTI-1223 up to 0.6 wt. % and grain begins to shrink above this value of percentage. The bulk sample $(\text{SnO}_2)_p/(\text{Cu}_{0.5}\text{Tl}_{0.5}\text{Ba}_2\text{Ca}_2\text{Cu}_3\text{O}_{10-\delta})$ EDXA gives the information of sitting between the grains at $p=0.2$ wt % of SnO_2 . Larger amount of nanoparticles SnO_2 results in decrease of porosity. With the increment of porosity from 0.0 to 0.4 wt. %, the grains information was found through SEM analysis.

Hermiz [9] Prepared samples of Mg-doped Bi-2223 superconducting materials. The composition of samples $\text{Bi}_{1-\delta}\text{Pb}_{0.4}\text{Sr}_2\text{Ca}_{2-x}\text{Mg}_x\text{Cu}_3\text{O}_{10+\delta}$ ($0 \leq x \leq 0.5$) were synthesized by solid state reaction method. The samples were characterized by x-ray diffraction which confirmed that the samples have an orthorhombic structure. She investigated that when Mg doped in Bi-2223 the structural and dielectric properties i.e. dielectric constant (real and imaginary part), dielectric loss and ac conductivity have a prominent dependence upon frequency. Also electrical resistivity was also affected by doping of Mg which sharply dropped with a transition temperature of 104 K. She observed that samples with $x = 0, 0.2, 0.5$ in dielectric measurements the capacitance has negative value at low frequency ranges.

Nadeem *et al.* [10] synthesized nickel/nickel-oxide $(\text{Ni}/\text{NiO})_x/(\text{CuTI-1223})$ nanoparticles superconductor by solid state reaction method. They investigated that with the addition of Ni/NiO nanoparticles, the structural and superconducting properties of host copper thallium

matrix were affected. The samples were characterized by XRD, SEM and EDX. By using these techniques the structural, morphological and compositional properties were studied. The critical temperature (T_c) has decreased with the addition of nanoparticles in host materials. The superconducting parameters have also reduced by the addition of core-shell Ni/NiO nanoparticles without any significant change in structure and cell parameters.

Mumtaz *et al.* [11] synthesized the $(\text{CuO}, \text{CaO}_2, \text{ and BaO})_y/\text{CuTi-1223}$ superconductor composites by solid-state reaction method. These composites were studied under different temperature and frequency ranges. They characterized the samples by XRD, SEM, RT measurement and FTIR. The dielectric properties were approved by LCR meter in different temperature and frequency ranges i.e. 78 to 300 K and 10 kHz to 10 MHz, respectively. They observed that by the addition of nanoparticles the structure of superconductor remain unchanged. Also by the SEM results the inter-grain connectivity is improved after the addition of nanoparticles. They observed that dielectric properties were strongly temperature and frequency dependent. The ac-conductivity (σ_{ac}) and frequency ranges of superconductor composites were also steadily increased.

Dou *et al.* [12] investigated that the doping has an effect of iron on the superconducting properties of MgB_2 because the Fe is main covering material for the manufacture of MgB_2 wires. They characterized by XRD which shows that iron doping was not effected on the lattices parameters of MgB_2 . They observed that by doping of iron nanoparticles the critical temperature and critical current density were decreased in both thin film and bulk form. They analyzed that iron nanoparticles combined with boron to form FeB and FeB_2 that are uniformly distributed within the matrix. The reduction in the value of current density by the doping of Fe is attributed to the decoupling effect of iron particles insides the grain boundaries.

Waqee-Ur-Rehman *et al.* [13] reported the infield superconducting properties of CuTi-1223 superconducting matrix with the addition of cobalt nanoparticles and characterized by different characterization techniques which are discussed in this article. XRD pattern shows that the structure of host CuTi-1223 matrix was unaltered after the addition of cobalt nanoparticles. These cobalt nanoparticles occupy the intergrain boundaries of the host CuTi-1223 and separation of intergrains weak links shows decrease in flux pinning. By increasing the concentration of Co nanoparticles the activation energy have been decreased. Also superconducting resistive transition broadening was investigated by the application of magnetic

field from 0-7 T. This property attributes to dissipation mechanism which is the cause of thermal activated flux flow (TAFF) by applying small amount of current which is 10 micro amperes. By increasing the value of magnetic field the rate of cobalt nanoparticles at grain sites slow down the decreasing of $U_0(H)$ which are helpful in high field application of superconductor.

Waqee-Ur-Rehman *et al.* [14] synthesized $(Ni)_x/CuTl-1223$ nano-superconducting composites and then characterized by different characterization techniques. XRD pattern shows that there is no variation in the crystal structure and cell parameters. Also the host CuTl-1223 is dominant and no change in the crystallite size of CuTl-1223 matrix after the addition of Ni nanoparticles. The in-field transport properties of CuTl-1223 phase were suppressed after the addition of Ni nanoparticles which may be attributed to weak flux pinning center. By applying external magnetic field the superconducting transition broadening was observed. Thermal activated flux flow was used to explain in-field dc resistivity. The vortex motion which rises due to external magnetic field from 0-7 T causes dissipation in $(Ni)_x/CuTl-1223$ nano-superconducting composites. The in-field superconducting properties were reduced by application of magnetic field which also decreases the $U_0(H)$ due to dissipation. By increasing the cobalt nanoparticles content and magnetic field increase the transition width ΔT and also give the suppression of pinning.

Irfan *et al.* [15] Synthesized $(Co)_x/CuTl-1223$ nano-superconductor composites and then studied by using different characterization techniques. There was no effect on the structure of host CuTl-1223 matrix. The addition of these nanoparticles suppressed the superconducting transport properties. The surface morphology shows that these nanoparticles occupy at grain boundaries. The suppression of superconducting properties leads to pair breaking across blocked ferromagnetic cobalt nanoparticles and superconducting volume fraction of CuTl-1223 matrix decreases. The normal state resistivity increases which attributes to magnetic moment of cobalt nanoparticles at grain boundaries of CuTl-1223 matrix and their spin alignment in particular direction. The diamagnetic signal of CuTl-1223 matrix was also decreased due to ferromagnetic cobalt nanoparticles.

References

1. Jabbar, I. Qasim, K. M. Khan, Z. Ali, K. Nadeem, and M. Mumtaz "Synthesis and superconducting properties of $(Au)_x/CuTl-1223$ composites" *J. Alloys Compd.* **618**, 110 (2015).
2. S. Cavdar, H. Koralay, and S. Altindal, "Effect of vanadium substitution on the dielectric properties of glass ceramic Bi-2212 superconductor" *J. Low Temp. Phys.* **164**, 102 (2011).
3. S. Cavdar, H. Koralay, N. Tugluoglu, and A. Gunen, "Frequency-dependent dielectric characteristics of Tl–Ba–Ca–Cu–O bulk superconductor" *Supercond. Sci. Technol.* **18**, 1204 (2005).
4. A. Jabbar, I. Qasim, M. Waqee-ur-Rehamn, M. Zaman, K. Nadeem, and M. Mumtaz, "Structural and superconducting properties of $(Al_2O_3)_y/CuTl-1223$ composites" *J. Electron. Mater.* **44**, 110 (2015).
5. N. H. Mohammad, "Effect of MgO Nano-oxide Addition on the Superconductivity and Dielectric Properties of $Cu_{0.25}Tl_{0.75}Ba_2Ca_3Cu_4O_{12-\delta}$ Superconducting Phase" *J. Supercond. Nov. Magn.* **25**, 45 (2012)
6. A. N. Jannah, R. Abd-Shukor, and H. Abdullah "Effect of Co_3O_4 Nanoparticles addition on (Bi, Pb)-2223 superconductor world academy of science, Engineering and Technology" *Int. J. Math. Comp. Phy. Elec. Com. Eng.* **7**, 3, (2013).
7. R. Awad, "Study of the Influence of MgO Nano-Oxide Addition on the Electrical and Mechanical Properties of $(Cu_{0.25}Tl_{0.75})-1234$ Superconducting Phase" *J. Supercond. Nov. Magn.* **21**, 461 (2008).
8. N. H. Mohammad, A. I. Abou-Aly, I. H. Ibrahim, R. Awad and M. Rkaby, "Mechanical properties of $(Cu_{0.5}Tl_{0.5})-1223$ added by nano- SnO_2 " *J. Alloys Compd.* **486**, 733 (2009).
9. G. Y. Hermiz, "Dielectric properties of $Bi_{1.6}Pb_{0.4}Sr_2Ca_{2-x}Mg_xCu_3O_{10+\delta}$ ($0 \leq x \leq 0.5$) superconducting system" *Int. J. Innov. Res. Sci. Eng. Technol.* **3**, 8564 (2014).
10. K. Nadeem, F. Naeem, M. Mumtaz, S. Naeem, A. Jabbar, I. Qasim, Nawazish A. Khan, "Synthesis and characterization of core-shell Ni/NiO nanoparticles/CuTl-1223 superconductor composites" *Ceram. Int.* **40**, 13819–13825 (2014).

11. M. Mumtaz, M. Kamran, K. Nadeem, Abdul Jabbar, Nawazish A. Khan, Abida Saleem, S. Tajammul Hussain, and M. Kamran, "Dielectric properties of (CuO, CaO₂, and (BaO)_y/CuTl-1223 composites" *J. Low Temp. Phys./ Fiz. Nizk. Temp.* **39**, 806 (2013).
12. W. X. Li, R. Zeng, L. Lua, Y. Zhang, S. X. Dou, Y. Li, R.H. Chen , M. Y. Zhu "Improved superconducting properties of in situ powder-in-tube processed Mg_{1.15}B₂/Fe wires with nano-size SiC addition" *Physica C*, **469**, 1519–1522 (2009).
13. M. Waqee-ur-Rehman, M. Mumtaz, Irfan Qasim, K. Ndeem "Infield response of (Co)_x/CuTl-1223 nanoparticles- superconductor" *J. Cryogenics* **73**, 68-72 (2016).
14. M. Waqee-Ur-Rehman, M. Mumtaz, Irfan Qasim, K. Ndeem " Infield superconducting properties of Ni nanoparticles added CuTl-1223 phase" *Solid State Commun.* **228**, 32-35 (2016).
15. Irfan Qasim, M. Waqeer-Ur-Rehman, M. Mumtaz and K. Nadeem, "Role of Co nanoparticles in CuTl-1223 superconductors" *Ceram. Int.* **73**, 78 (2016).

Chapter 3

Synthesis and Characterization Techniques

3.1 Synthesis of Nanomaterials

There are two types of approaches that we use for the synthesis of nanomaterials.

- ❖ Bottom up approach
- ❖ Top down approach

3.1.1 Bottom up approach

In this type of approach large and organized system is formed by the assembly of small components of atoms or molecular dimension. Common bottom up approaches commonly used are physical vapor deposition, chemical vapor deposition, electrochemical deposition molecular beam epitaxy and sol-gel method etc. Bottom up methods are described as additive technologies.

3.1.2 Top down approach

In this type of approach a small nano-sized structure is formed by the cutting of the bulk material. Common method that are used in this type of approach are lithography milling, ion etching. The synthesis of the nanoparticles and fabrication can be done by these two methods of approaches but the disadvantage in using the top down approach is imperfection of surface structure. Top down and bottom up approaches are shown in Fig. 3.1 [1].

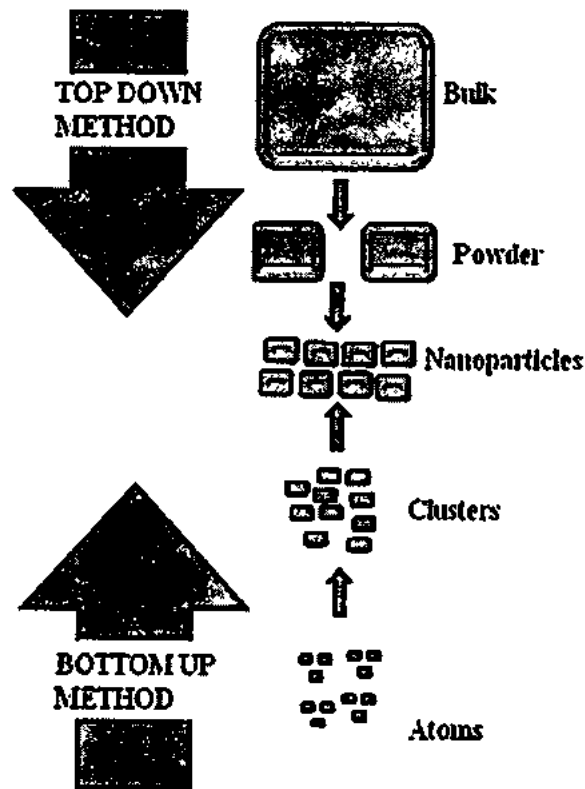


Fig. 3.1: Top down method vs. bottom up method [2].

3.2 Synthesis of Cobalt Oxide nanoparticles

I was interested to study R-T measurements of CuTl-based added with Co_3O_4 nanoparticles. We want to improve the superconducting properties of CuTl-1223 matrix by adding nanoparticles. So I worked on $(\text{Co}_3\text{O}_4)_x/(\text{Cu}_{0.5}\text{Tl}_{0.5})\text{Ba}_2\text{Ca}_2\text{Cu}_3\text{O}_{10-\delta}$ nano-superconductor composites with different wt.% of Co_3O_4 nanoparticles. Fig. 3.2 shows the schematic diagram to form Co_3O_4 nanoparticles using sol-gel method.

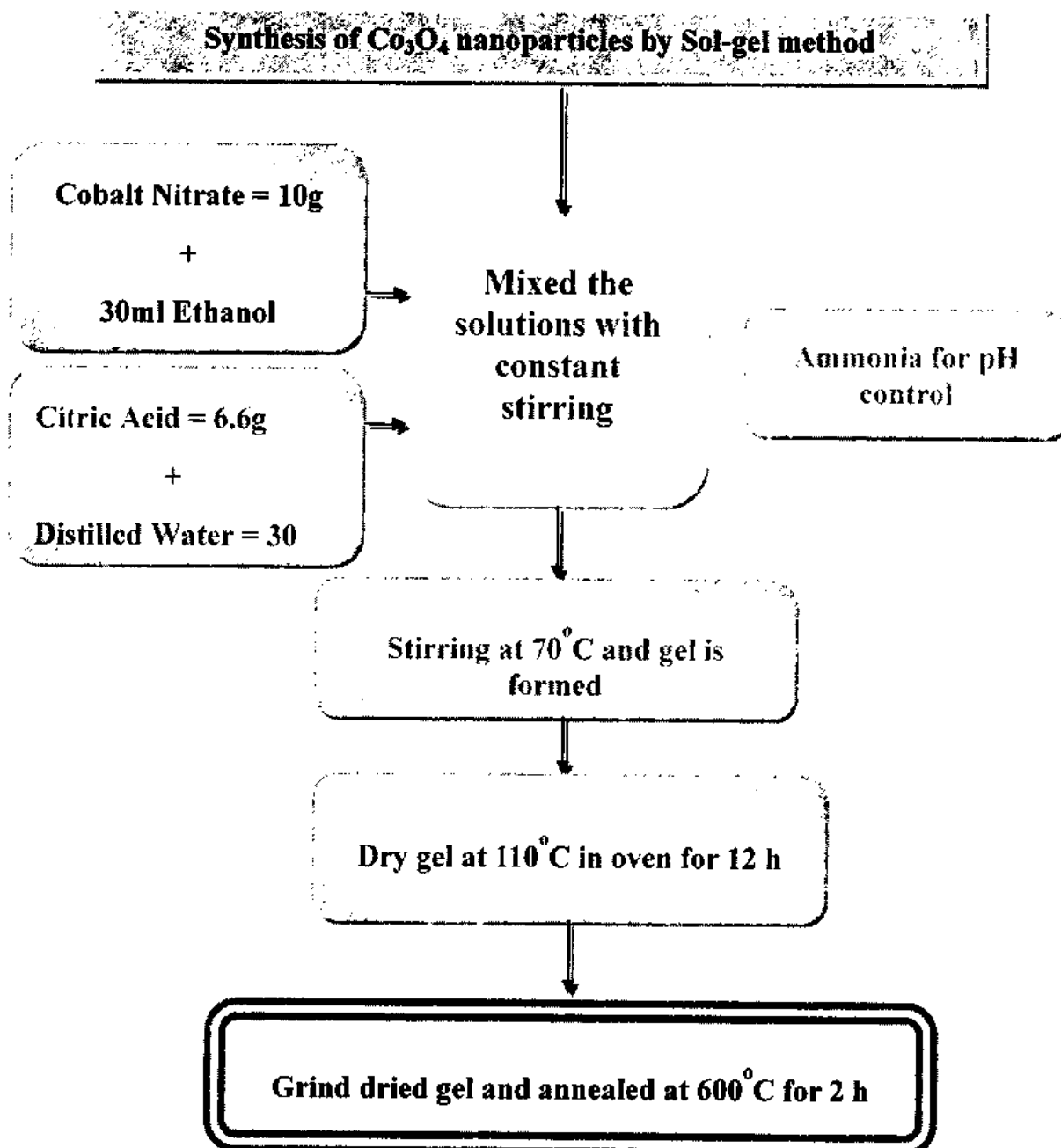


Fig. 0.2: Flow chart for the synthesis of Co_3O_4 nanoparticles by sol-gel method.

3.3 Preparation of $(\text{Co}_3\text{O}_4)_x/\text{CuTi}$ -based nano-superconductor composites

The bulk superconductor $(\text{Cu}_{0.5}\text{Ti}_{0.5})\text{Ba}_2\text{Ca}_2\text{Cu}_3\text{O}_{10-\delta}$ was prepared by using solid state reaction method as indicated in the flow chart below. $\text{Cu}_2(\text{CN})_2\text{H}_2\text{O}$, $\text{Ba}(\text{NO}_3)_2$, $\text{Ca}(\text{NO}_3)_2\cdot 4\text{H}_2\text{O}$ compound were the initiative chemicals to prepare bulk precursor material. These chemicals were mixed according to a suitable amount after calculations in an agate mortar and pestle for 2 hours. After grinding the mixed material was placed in quartz board and fired at 860°C for 24 hours in chamber furnace with following the cooling at room temperature. The flow chart for the preparation of precursor material is shown in Fig. 3.3. The firing step was again repeated after grinding of 2 hours but the material was placed in ceramic board. Ti_2O_3 was mixed with the obtained sample according to required wt% in order to obtain the superconductor compound i.e. CuTi-based. In our project we added appropriate wt. % (x) of Co_2O_3 nanoparticles to obtain $(\text{Co}_3\text{O}_4)_x/\text{CuTi}$ -based superconductor (where $x = 0, 0.25 \text{ wt.}\%, 0.50 \text{ wt.}\%, 1.0 \text{ wt.}\%$ and $2.0 \text{ wt.}\%$). After mixing, the material obtained was pelletized under 3.8 tons/cm^3 pressure and the pellets obtained were wrapped in gold capsules before heated at 860°C for 10 minutes. After heating, it was allowed to quench to room temperature and nano-superconductor is formed is shown in Fig. 3.4.

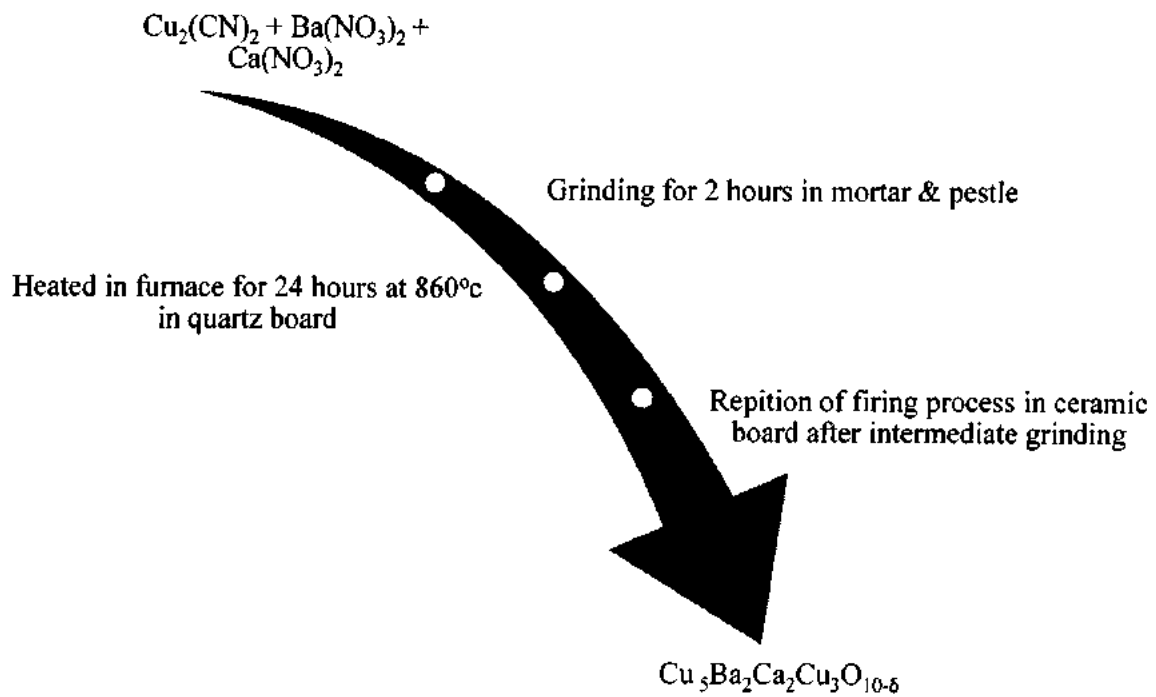


Fig. 3.3: Flow chart for the preparation of superconductor precursor material.

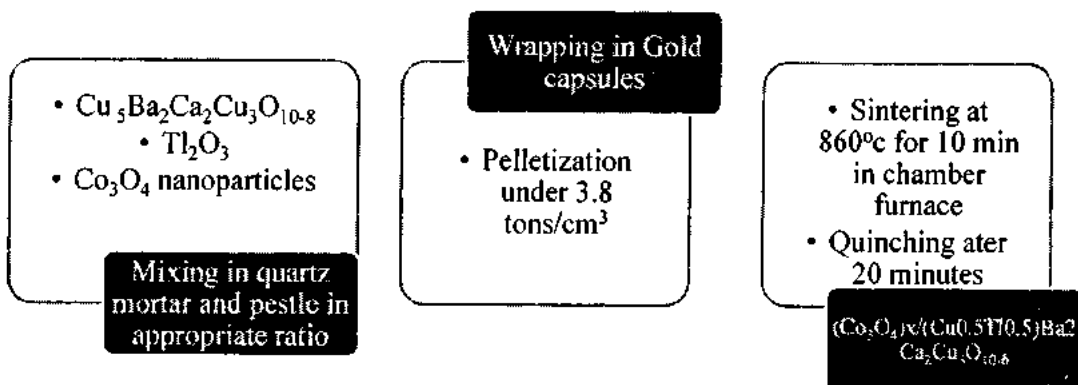


Fig. 3.4: Flow chart for the synthesis of $(\text{Co}_3\text{O}_4)_x/\text{CuTI-1223}$ nano-superconductor composites.

3.4 X-ray diffraction (XRD)

In order to determine the crystal structure of a solid and crystallite size the most popular and common technique used to sense these issues is called x-ray diffraction (XRD). The structure, geometry and lattice parameters of crystals can be studied by using XRD. This technique is commonly used to identify the defects, structures of unknown materials and stresses present in the crystals. In 1895, a German physicist Roentgen noticed a flash of light emitted from the sheet of the paper coated with barium platinocyanide when he was working on the luminous property of certain materials based on some conducting tests as result of cathode rays. After performing certain experiments he drew a conclusion that when the cathode rays strike the target material they emit invisibles and penetrating radiations. At that time there was no information about the nature of these rays and so Roentgen gives the name called as X-rays. [3].

The regular arrangement and well-ordered repetition of atoms in space is called crystal lattice. The lattice composed of three interatomic spacing and interfacial angles as shown in Fig. 3.5. The crystalline lattice determines the structural properties of a material.

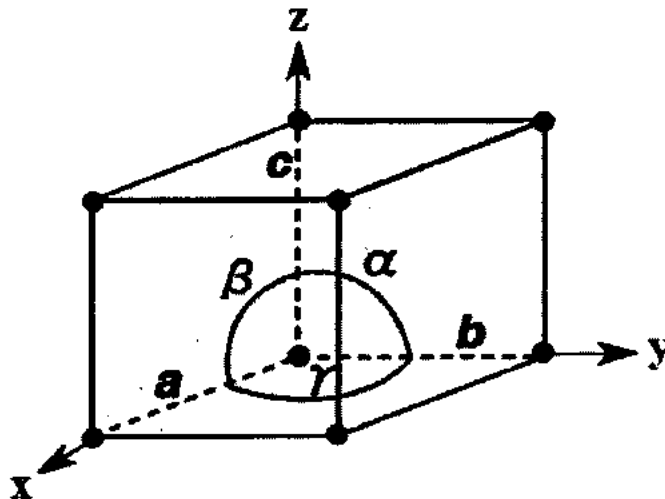


Fig. 3.5: Lattices shape with angles and lengths [4].

These X-rays are electromagnetic radiations that's have very short wavelength i.e. 1 \AA or 10^{-10} m . Since X-rays have very shorter wavelength which is comparable to interatomic spacing of crystals so they are suitable for diffraction techniques. The diffraction of X-rays is used to determine the arrangements of atoms, structure of the materials, bonding force of atoms and their arrangements in lattice. Crystallite size and interatomic distances are also determined

by using this technique. The unknown materials can be identified by comparing the XRD pattern of the unknown materials with reference pattern of the materials. The information about the type of materials i.e. crystalline and amorphous can be obtained through this technique. The diffraction pattern of the materials can be obtained by using X-rays diffractometer which is shown in Fig. 3.6 [5]. The XRD consists of various parts which are given below;

- X-ray tube which is used to produce X-rays
- Sample chamber which is used to place the sample
- X-rays intensity can be measured by using Scintillation counter
- Measuring device used to measure angle
- To cool X-rays tube chiller with cooled water can be used
- The output can be recorded by the computer

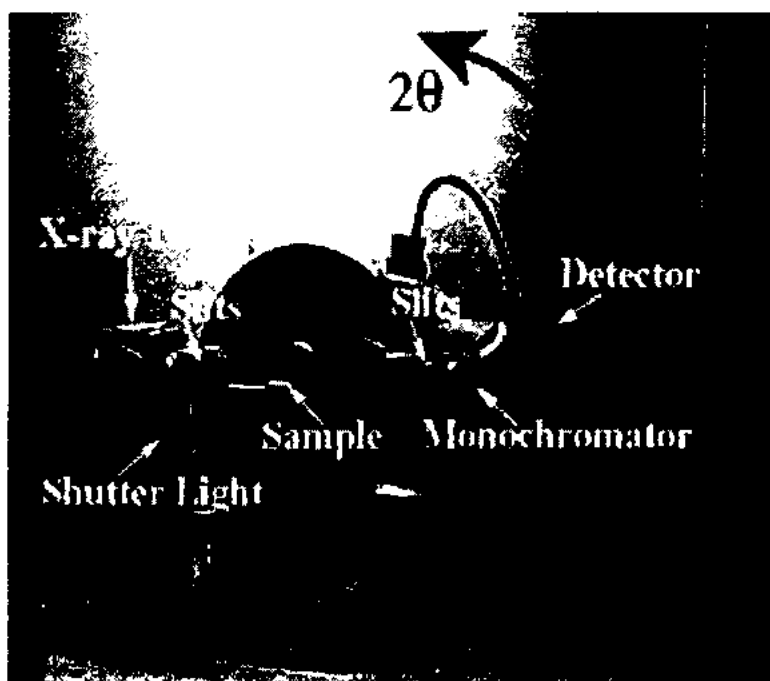


Fig. 3.6: A typical X-ray diffractometer [6].

X-rays are produced inside the sealed tube which is at high vacuum which is placed inside the X-ray diffractometer. X-rays are bombarded on the target material which is usually made of molybdenum or copper. A high voltage source i.e. 15-60 kV is used to accelerate the X-

rays beam which strikes the filament due to which it is heated and electrons emit through it. As result transition takes place in the inner shell of target materials. K-shell is ionized by the beam of electrons and as result electrons jump from higher energy states to fill this K-shell vacancy and as a result a photon of x-ray emitted whose energy is hf . These X-rays which are emitted due to transition are focused with high accuracy on the sample. After X-rays are incident on the sample and after interacting with the atoms of the samples are diffracted at angle θ . The typical mechanism of Bragg's law is shown in the Fig. 3.7. The X-rays will be diffracted from the sample that is satisfying in the Bragg's law or their wavelength is comparable with the interatomic distance of the sample that is given in below,

$$2d\sin \theta = n\lambda \dots \dots \dots (3.1)$$

In the above equation, λ shows wavelength of incident X-rays, d shows interatomic distance, and θ is the angle of incident X-rays beam. The angle θ can be calculated from Brags equation with the help of given valves of wavelength of incident X-rays. Where, n is called the order diffraction and $n = 0, 1, 2, 3 \dots$. In case of polycrystalline composite that consists tiny crystal the powder diffraction technique is typically used [7]. The diffraction of X-rays helps to find out intensive crystal like peaks in a crystal due to regular arrangement of lattices. The sample is placed in the path of monochromatic x-rays beam at a particular angle θ the wavelength is kept constant and interplanar spacing d and θ are changed. By using this analysis bending angles, dimension of unit cells and typography of planes can be determined. This technique is commonly used in all fields of material science, engineering sciences, biological science and medicines as well as in environmental sciences. Avery small amount of material is used in this technique for structure analysis and crystallite size etc.

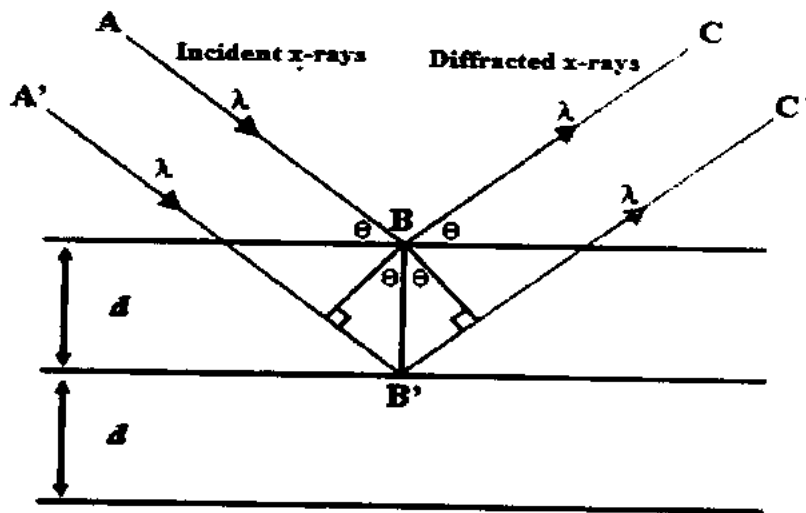


Fig. 3.7: Schematic diagram of Bragg's law [8].

The X-rays wavelength λ , interatomic distance d and angle of diffraction θ are related with each other as in Bragg's law. The XRD pattern obtained from characterization technique of XRD can be analyzed further by the comparison of different charts of the materials and then its crystallite size can be calculated by using Scherrer's formula which is given bellow,

$$D = K\lambda/\beta\cos\theta \dots \dots \dots (3.2)$$

In the above equation D shows the crystallite size of the particles, θ is angle of diffraction and β is full width half maxima (FWHM). Also 'K' represents a shapeless factor having value 0.9 known as Scherrer's constant and it depends upon the shape of the crystal. A computer program is used to analyze the obtained data from XRD analysis. Different peaks are obtained which can be related with existing and organized crystal structure [9].

3.5 Scanning Electron Microscope

Scanning electron microscope (SEM) is surface sensitive imaging technique that gives information about the surface morphology of the material. Normally, this technique is not applicable to give the material bulk information. Similarly, this technique is a wide source to identify the weak-links, voids and pores of the surface. The specimen depth of the ejected secondary electron is 3 to 10 nm. When primary beam of electrons are bombarded from tungsten filament, having energy 500 eV to 60 keV, these primary electrons are combined to anode from where they are received on magnetic lenses. The Lorentz force acting on these electron to accelerate towards the scanning coils. The scanning coil expel extra undesired beam and required

beam is then hit on the sample. Different electrons like secondary electron, back-scattered electron, auger electron and X-rays are ejected from the surface of the sample which gives information of the surface structure [10]. Usually, 95% of surface information can be taken from secondary electrons and these electrons are easily to control and detect on the detector as shown in Fig. 3.8.

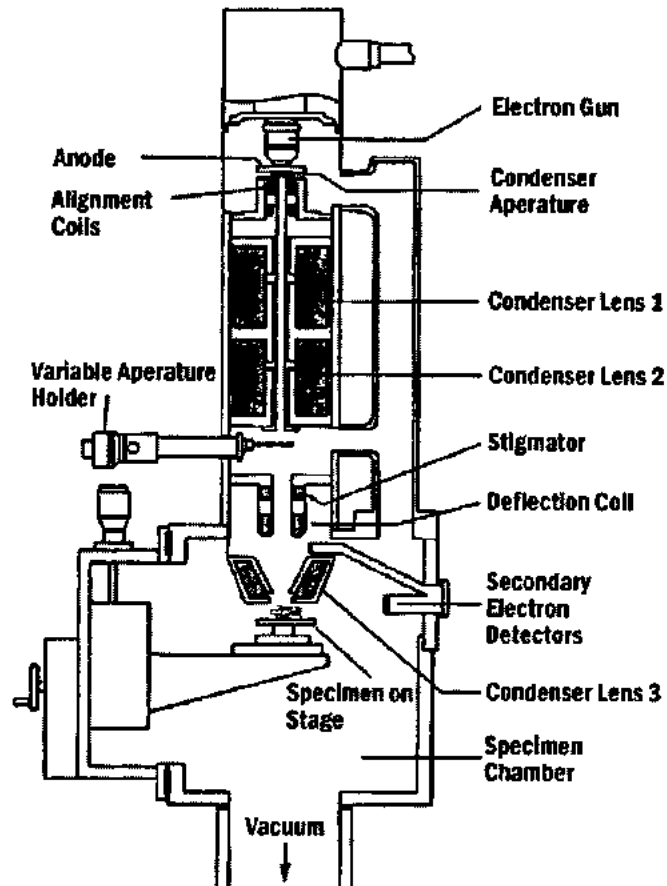


Fig. 3.8: Schematic diagram of SEM [11]

3.5.1 Secondary electrons

These electrons are easily controllable and because they have energy of 500 eV. When these electrons are detected, a magnifier magnifies the images of this electron and converted from analogue to digital converter and stored for further investigation on the storage.

3.5.2 Backscattered electrons

These are originally primary electrons that reflect back from the sample with 180°. These are also the source of surface as well as for the bulk information of the material but due to high energy, these electrons are very difficult to control on ordinary secondary electron detector. A special type of detectors is designed for the detection of these electrons [12].

3.5.3 Auger electrons

When primary electrons hit on the sample atoms, electrons are knock out from the orbit. Another orbit electron fills this vacancy and photon (of energy difference between these two orbits) is emitted. This photon when collide with other electron within the atom, this electron is ejected and known as auger electron which has information of material from which it is ejected. They escape from the region which is closed to the surface. The information about the chemical composition of the sample is provided by the auger electrons having energy which depends upon the structure of the atoms [13]. The schematic diagram is shown in Fig. 3.8.

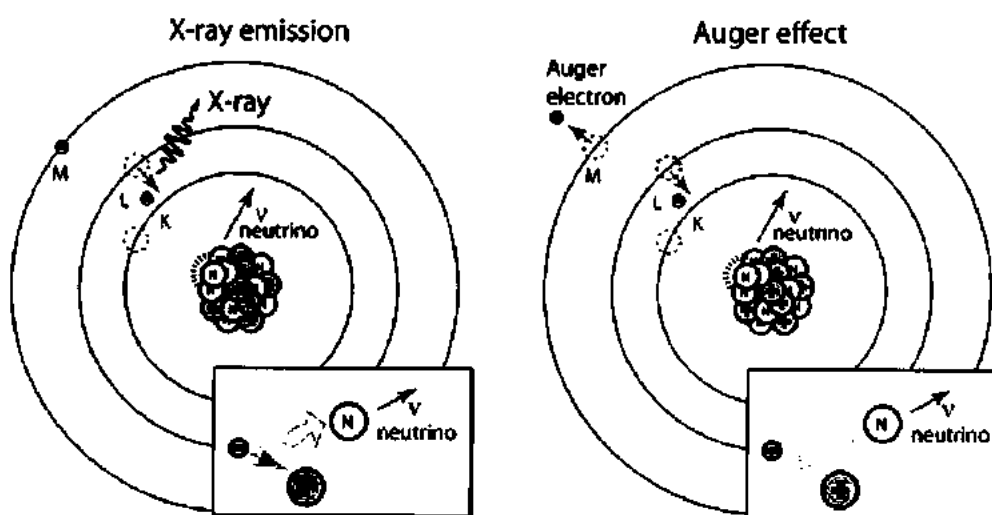


Fig. 3.9: Emission of auger electrons and X-rays from the sample [14].

3.5 Fourier Transform Infrared (FTIR) spectroscopy

The infrared spectroscopy is the study of electromagnetic radiations and also its contact with matter that can be studied by using infrared region. In IR region the electromagnetic radiations are related with the vibrations of molecules. These IR radiations are bombarded on the target materials. These radiations that are bombarded on the target sample can be absorbed and transmitted by the sample. When IR radiation is absorbed by the sample it can be excited to higher energy states by absorbing infrared radiations. Generally a huge amount of energy can be absorbed by the sample if the energy of the photon matches with the vibrational energy levels. If the IR radiations contact with the molecules and also change occur in molecular dipoles the absorption of IR radiations will be take place [15]. When the IR radiations incident on the specimen the molecules absorb as well as transmit the radiations which is shown by spectrum or interferogram. This analysis can make FTIR as a valuable tool for various types of investigation and characterizations. The information about the chemical composition of the compositions can be provided by infrared spectroscopy in the light of the above facts. XRD results and identity of unknown material can be conforms by IR spectroscopy and also the quality of the specimen and components quality in a substance can be justified by FTIR. The specimen spectrum can be obtained by FTIR spectrometer through interferogram and this spectrum of the specimen can be analyzed through the application of FTIR interferogram. The basic principle of FTIR spectrometer can be based on Michelson interferometer which is shown in Fig. 3.10 [16].

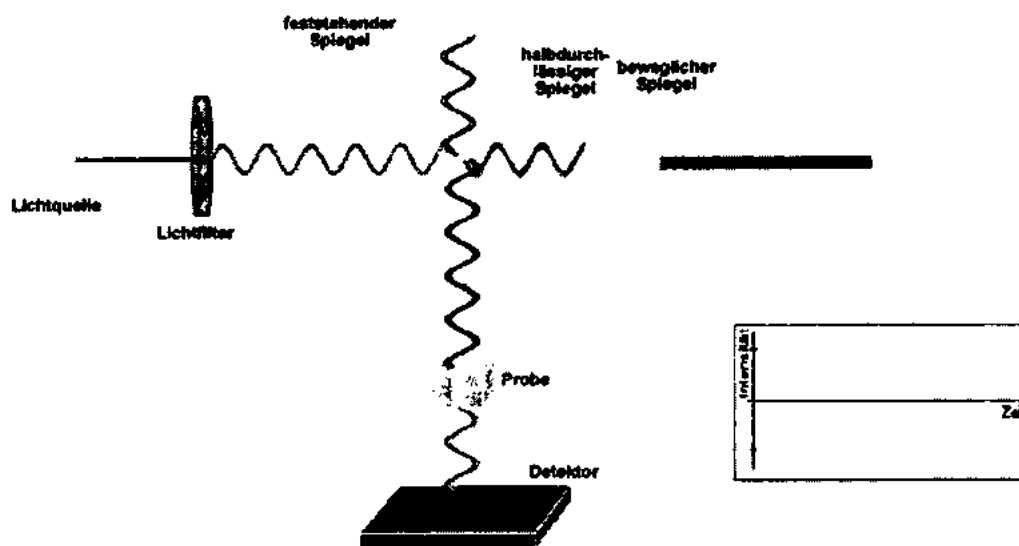


Fig. 3.10: Michelson interferometer [17].

The little amount of the sample is mixed with KBr. By grinding the mixture the resultant mixture is made homogenous and then the pallets of the resultant mixture can be made. The KBr pallets give the background spectrum and then spectrum of the specimen can be noticed through it. The spectrometer's resolution is adjusted in such a way that it can take the number of scans of the specimen within 400 to 700cm^{-1} . The numbers of scans were taken from 10 to 75. By the help of spectrometer the background spectrum was subtracted and after that the specimen spectrum was noticed.

3.6 Resistivity measuring technique

Physical property measurement system (PPMS) used for temperature dependent resistivity measurement. PPMS used to find the temperature at which the resistance of the superconductor is vanished. The alteration in critical parameters of superconductor such as T_c is observed before and after the addition of nanoparticles through this technique. The formation of resistivity in a material is the contribution of interaction between electrons, imperfections as well as lattices vibrations. Four probe methods are used to perform these tasks [18]. In order to measure the resistivity of a sample, four wires 1, 2, 3 and 4 are connected with one another. A specimen is covered with silver paste to make it conductive and also to make connection between wires and specimen. These wires are connected with each other at equal distance and in straight line and the probes that meet at same points with the sample as shown in Fig. 3.11.

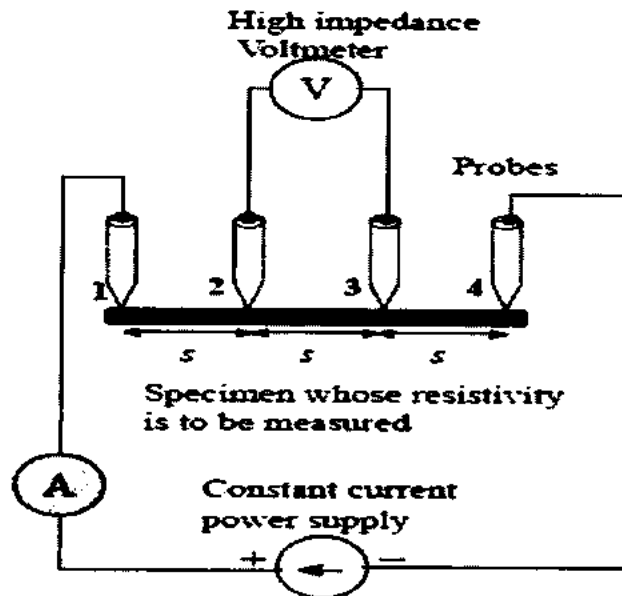


Fig. 3.11: Four-probe method [19].

All the four wires are connected with AC current supply in which two end wires hold non varying current. For better results the size of the specimen should be in millimeter ranges. The voltage drop V is calculated by using ohm law along the probes that is 1 and 4 that contain non varying current and contact 2 and 3 containing varying current. Also ammeter and voltmeter are also used in this experimental setup is shown in Fig. 3.12. In case of superconductor the contacts are implemented on the specimen and then the specimen is dipped in to the liquid nitrogen having boiling point of about 77 K or liquid helium [20]. By using the mathematical relationship between the resistivity ρ , cross sectional area A , length L and resistance R can be written as,

$$R = \rho L/A \dots \dots \dots (3.3)$$

In this equation, the value of R is putted by using ohm law and then the resistivity can be calculated

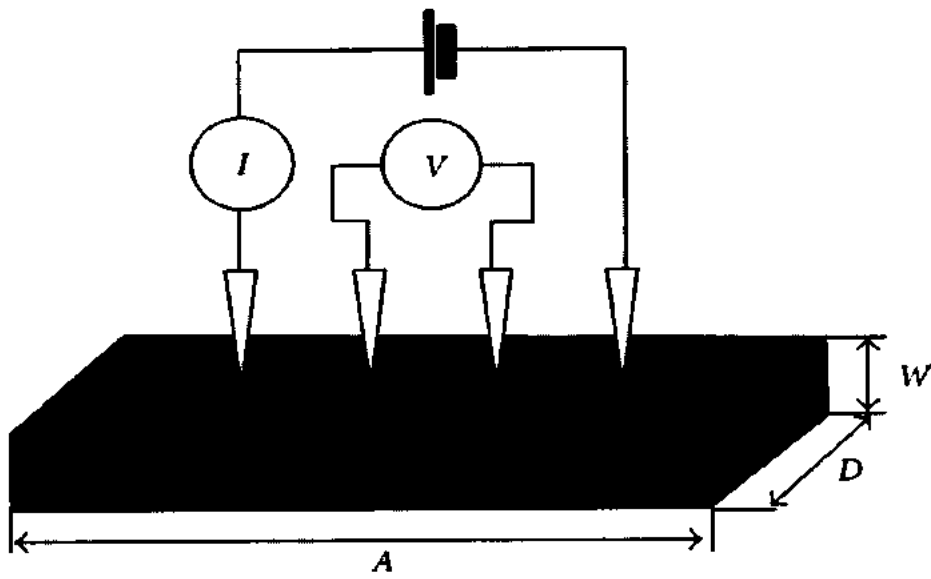


Fig. 3.12: Demonstration of contacts of wire on specimen [21].

References

1. K. J. Klabunde, L. Erickson, O. Koper, and R. Richards, "Review of Nanoscale Materials in Chemistry: Environmental Applications" ACS Symp. Ser. **1045**, 1-13 (2010).
2. <http://www.pharmainfo.net/book/emerging-trends-nanotechnology-pharmacy-1introduction-nanotechnology/techniques-convert>
3. J. D. Aiken III, and R. G. Finke, "A Review of Modern Transition-Metal Nanoclusters; Their Synthesis, Characterization and Application in Catalysis" J. Mol. Catal. A. Chem. **145**, 1-44 (1999).
4. http://www.doitpoms.ac.uk/tlplib/crystallography3/images/lattice_parameters.gif
5. D. Vollath, "Nanomaterials: An Introduction to Synthesis, Properties and Applications" 2nd Ed. Wiley, Weinheim (2013).
6. <http://www.doitpoms.ac.uk/tlplib/xray-diffraction/images/labelled.jpg>
7. G. Cao, and Y. Wang, "Nanostructures and Nanomaterials: Synthesis, Properties, and Applications" 2nd Ed. Imperial College Press, London (2004).
8. <http://www.analyticalchemistrygsu.com/2013/03/braggs-law-with-applications-and.html>
9. L. Cademartiri, and G. A. Ozin, "Concepts of Nanochemistry" Wiley, Morlenbach (2009).
10. R. West, "Solid state Chemistry and Its Applications" 2nd Ed. Wiley (2014).
11. <http://emrf.research.uiowa.edu/scanning-electron-microscopy>
12. Guozhong Cao, University of Washington, USA, "Nanostructures & Nanomaterials, synthesis, properties & applications" Imperial College Press, UK. 2004.
13. V. Rajendran, A. Marikani, "Material Science, Core Engineering Series" Tata McGraw-Hill, 2004.
14. <http://hyperphysics.phy-astr.gsu.edu/hbase/nuclear/radact2.html>
15. G. B. S. Narang, and R. C. Gupta, "Materials Science" 7th Ed. Khanna, New Delhi (1993).
16. R. K. Sharma, B. Tiwari, and J. S. Tomar, "Study of Thermal Stability of Metal Carbon Nanotubes by SEM, XRD & TGA" Int. J. Innov. Res. Sci. Eng. Technol. **3**, 9081 (2014).
17. <http://alfa-img.com/show/michelson-interferometer-animation.html>
18. H. Ibach and H. Luth, "Solid State Physics: An Introduction to Theory and Experiment" Springer-Verlag (1991).
19. <http://amrita.vlab.co.in/?sub=1&brch=282&sim=1512&cnt=1>

20. H. Ibach, H. Lüth, "Solid State Physics: An Introduction to Principles of Materials Science", 2nd Edition, Springer (1995).
21. <http://www.hindawi.com/journals/jnm/2011/606714.fig.002.jpg>

Chapter 4

Results and Discussion

$(\text{Cu}_{0.5}\text{Tl}_{0.5})\text{Ba}_2\text{Ca}_{n-1}\text{Cu}_n\text{O}_{2n+4-\delta}$ ($n = 2, 3, 4, \dots$) is one of the most promising and remarkable family of the (HTSC). It has low anisotropy, long coherence length along c-axis, and high critical current density (J_c). The effects of different doping in thallium-based have been investigated. Nanoparticles addition effects in recently discovered MgB_2 superconductor showed great improvement in flux spinning [1].

4.1 X-Ray Diffraction (XRD)

The average crystalline size is calculated by Debye Scherrer's formula,

$$D = \frac{K\lambda}{\beta \cos\theta} \dots\dots\dots(4.1)$$

where 'K' is the Scherer constant and its value is 0.9, ' λ ' is X-rays wavelength ' β ' is the full width at half maximum, ' θ ' is the diffraction angle [2].

4.2.1 XRD Analysis of Co_3O_4 Nanoparticles

XRD scans of Co_3O_4 nanoparticles indicating sharp peaks are shown in Fig. 4.1. The peaks at $2\theta = 31.25^\circ, 36.89^\circ, 44.92^\circ, 49.16^\circ, 55.74^\circ, 59.44^\circ, 65.41^\circ, 69.31^\circ, 77.35^\circ$ were indexed to (022), (113), (004), (133), (224), (333), (044), (006), (335) planes of cubic structure of cobalt oxide nanoparticles, which follows $R\bar{3}m$ group. The average crystalline size of the Co_3O_4 nanoparticles is calculated by using Debye-Scherrer's formula. The average crystalline size of the Co_3O_4 nanoparticles is 71 nm [3]. The highest peak (113) give average crystallite size equal to 57 nm. The highest peak is due to the Co_3O_4 phase which identifies the formation of Co_3O_4 nanoparticles. There are no peaks of impurity or other phases were found in this XRD spectrum [4].

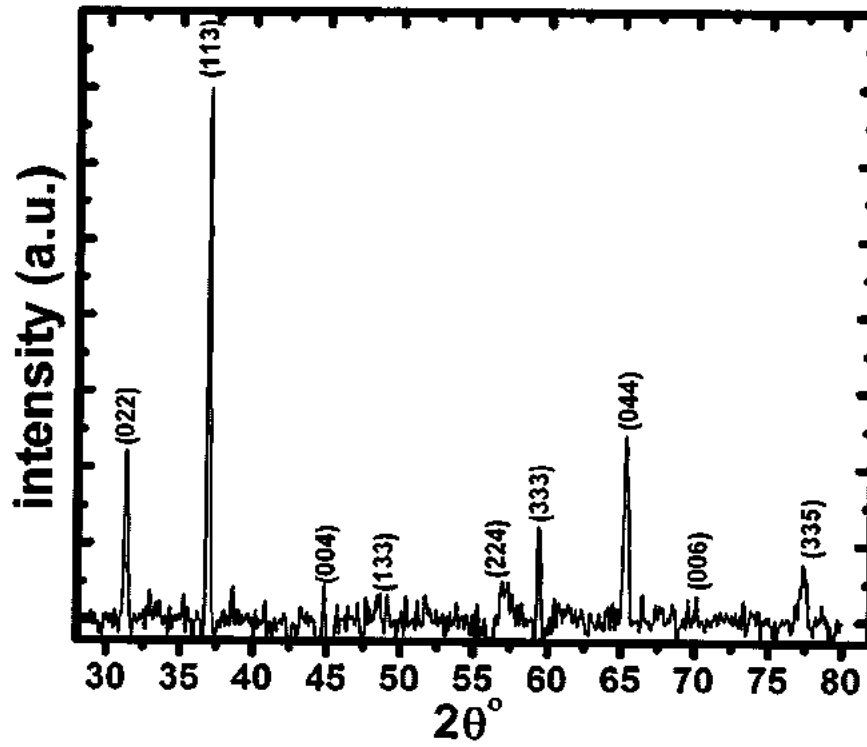


Fig. 4.1: XRD spectrum of cobalt oxide (Co₃O₄) nanoparticles.

4.2.2 XRD Analysis of Nano-Superconductor Composites

XRD patterns of (Co₃O₄)_x/CuTl-1223 nano-superconductor composites with different concentration of Co₃O₄ nanoparticles with $x = 0.0, 0.25, 0.50, 1.0$ and 2.0 % are shown in Fig. 4.2. The domination of CuTl-1223 phase is seen from these diffraction patterns, as most of the diffracted peaks are indexed in accordance to CuTl-1223 tetragonal structure, which follows P4/mmm group. Some un-indexed peaks of low intensity show the impurities or any other superconducting phases. These peaks were indexed by using computer software “check cell” [5]. The addition of Co₃O₄ nanoparticles in CuTl-1223 superconductor matrix does not significantly change the structural symmetry and the cell parameter of bulk CuTl-based superconductor [6,7]. The intensity of diffraction peaks reduces by increasing the concentration of nanoparticles which is due to decrease in the volume fraction of the overall superconducting bulk material [8,9].

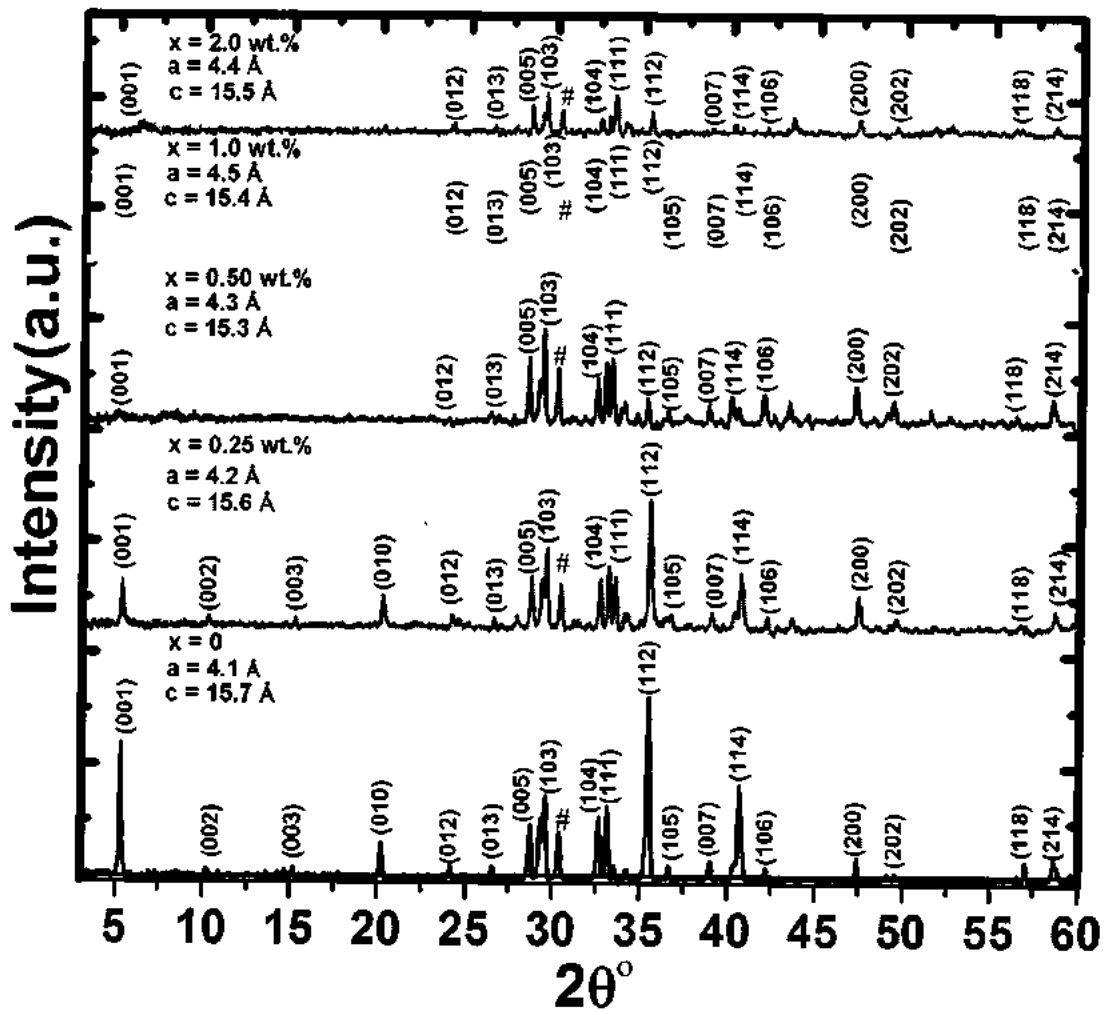


Fig. 4.2: XRD spectra of $(\text{Co}_3\text{O}_4)_x/\text{CuTI-1223}$ with $x = 0, 0.25, 0.50, 1.0$ and 2.0 wt.%.

4.3 Scanning electron microscopy (SEM)

Fig. 4.3 (a) and (b) shows the scanning electron microscopy images of bulk CuTI-1223 superconductor matrix at 10 and 5 μm scales. They show that the CuTI-1223 has granular structure with voids present in it. These voids can be filled by adding nanoparticles.

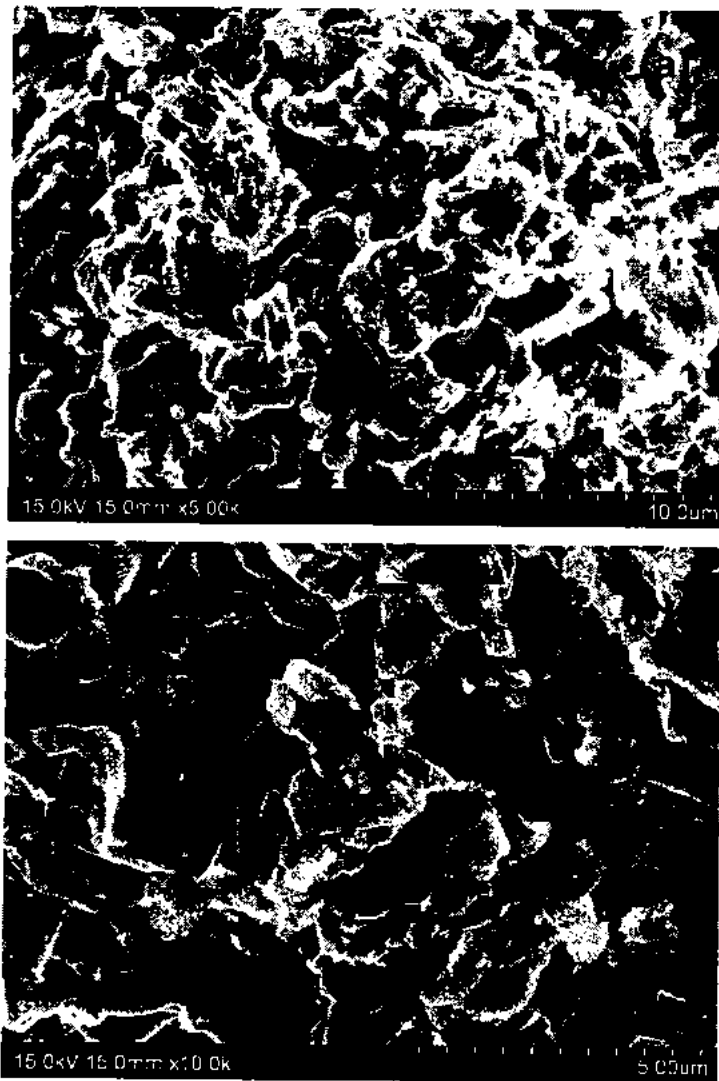


Fig. 4.3: SEM images of bulk CuTi-1223 superconductor matrix at (a) 10 μm and (b) 5 μm.

4.4 Fourier transforms infrared (FTIR) spectroscopy

FTIR is an experimental technique which gives information of different vibrational modes. Our interest is in different oxygen phonon modes which have important contribution in superconducting phenomenon. The FTIR absorption spectra of $(\text{Co}_3\text{O}_4)_x/\text{CuTi-1223}$ nano-superconductor composite with $x = 0.0, 0.25, 0.50, 1.0, 2.0$ wt.% in the far infrared range $400\text{-}700\text{ cm}^{-1}$ are shown in Fig. 4.4. FTIR spectra show the vibration of multiple oxygen atoms exhibited by the unit cell of superconductor. Apical oxygen, planner oxygen and O_8 atoms correspond to the bands ranging from 400 cm^{-1} to 540 cm^{-1} , 541 cm^{-1} to 600 cm^{-1} and 670 cm^{-1} to 700 cm^{-1} , respectively. The Co_3O_4 band is fused in the band of superconducting bands in the ranges $500\text{-}540\text{ cm}^{-1}$ [10,11]. The FTIR results show slight variation in the apical oxygen modes as well as in CuO_2 planner oxygen modes. While there is almost no change observed in O_8 oxygen modes. The variation in position of these oxygen vibrational phonon modes may be due to stresses and strains produced after cobalt oxide nanoparticles addition in CuTi-1223 matrix. FTIR and XRD findings verify that the unit cell of CuTi-1223 superconductors remains unchanged with the addition of nanoparticles and also these nanoparticles added to CuTi does not substrates the unit cell that lies the grain boundaries of the superconductors [12-14].

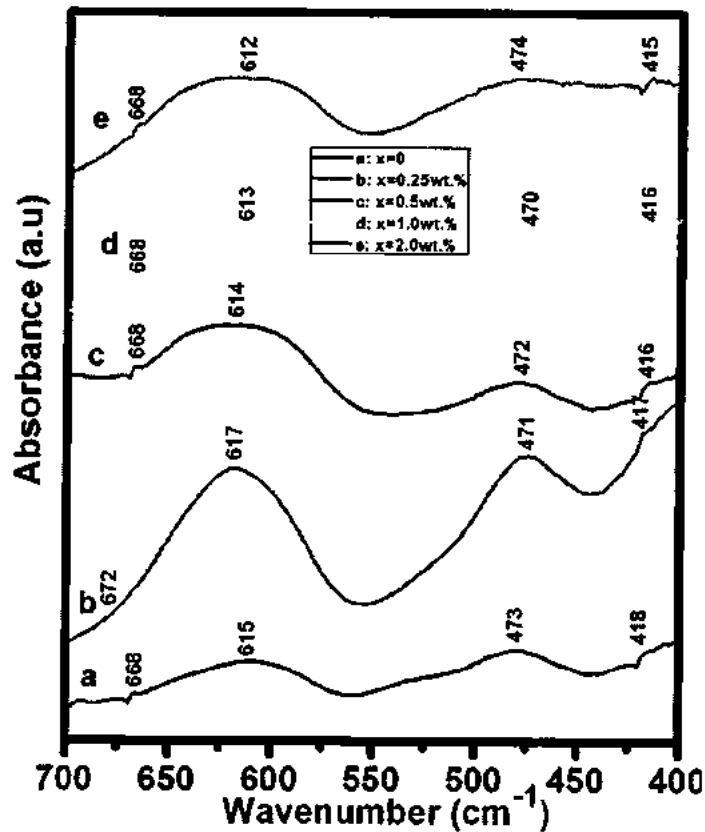


Fig. 4.4: FTIR spectra of $(\text{Co}_3\text{O}_4)_x/\text{CuTi-1223}$ with $x = 0, 0.25, 0.50, 1.0$ and 2.0 wt.%.

4.5 Resistivity measurements

Fig. 4.5 shows the resistivity (ρ) versus temperature (T) measurements of $(\text{Co}_3\text{O}_4)_x/\text{CuTi-1223}$ nano-superconductor composite samples with $x = 0.0, 0.25, 0.50, 1.0$ and 2.0 wt.%. The zero resistance critical temperature $\{T_c (R=0)\}$ comes out 105 K, 92 K, 81 K, 70 K and 40 K for $x = 0.0, 0.25, 0.50, 1.0$ and 2.0 wt.%, respectively. The cause of the T_c decrease can be the electrons scattering/localization due to these antiferromagnetic magnetic nanoparticles. When these magnetic Co_3O_4 added at grain boundaries, low porosity and the facilitation of mobile free carriers are showed by the decrease in temperature. These measurements show that the superconducting properties of CuTi-1223 matrix are decreased after the addition of Co_3O_4 nanoparticles [15].

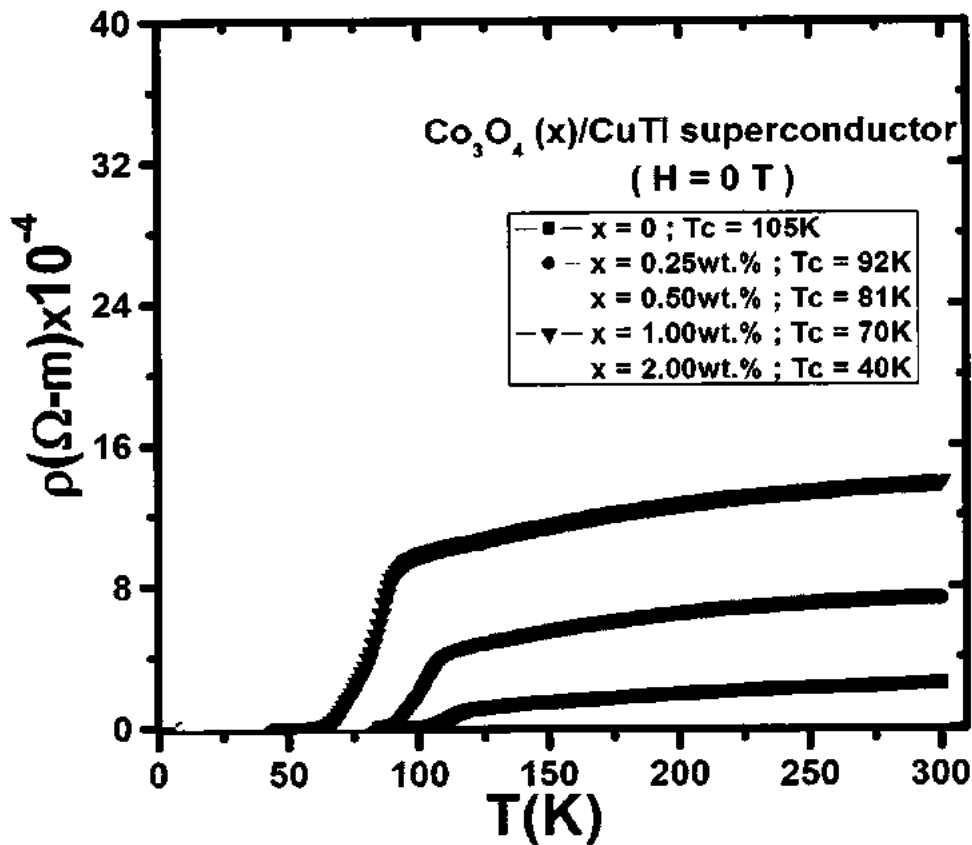


Fig. 4.5: RT measurements of $(\text{Co}_3\text{O}_4)_x/\text{CuTi-1223}$ composites with $x = 0, 0.25, 0.50, 1.0$ and 2.0 wt. %.

The variation of T_c with increasing concentration of Co_3O_4 nanoparticles is shown in Fig 4.6. The transition temperature decreases with increasing the concentration of Co_3O_4 nanoparticles. The superconducting properties gradually and systematically suppressed by increasing the concentrations of Co_3O_4 nanoparticles. The suppression of superconducting properties of $(\text{Co}_3\text{O}_4)_x/\text{CuTi-1223}$ composite after the addition of Co_3O_4 nanoparticles is most likely due to reduction in carriers density in the CuO_2 planes of the host CuTi-1223 . The oxygen affinity of Co_3O_4 nanoparticles creates oxygen vacancy disorder and ultimately reduces the carrier's concentrations in superconducting planes. After the inclusion of Co_3O_4 nanoparticles, the superconducting volume fraction and density of mobile charge carriers have decreased, which cause the suppression of superconducting parameters [16,17].

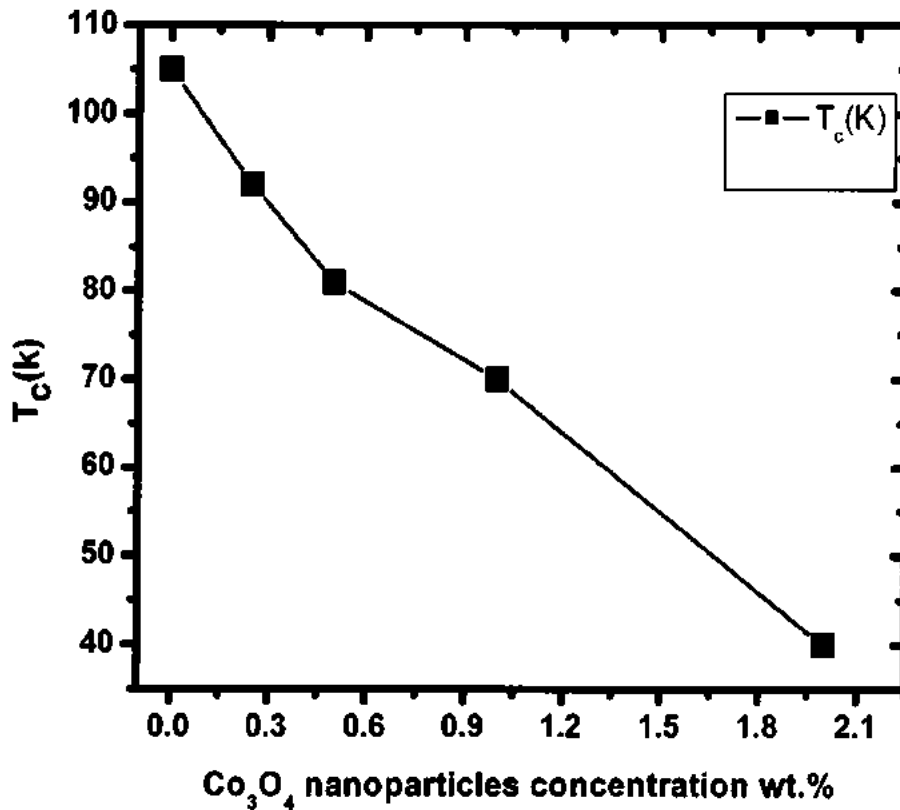


Fig. 4.6: Variation of critical temperature with concentration of Co_3O_4 nanoparticles in $(Co_3O_4)_x/CuTi-1223$ nano-superconductor composites.

Fig. 4.7 shows the variation of normal state resistivity with increasing nanoparticles concentration. The normal state resistivity increases by increasing the concentration of magnetic nanoparticles which may be due to scattering of superconducting electrons from these nanoparticles at the grain boundaries. The normal state resistivity is very high for the sample with $x = 2.0$ wt.%, which is the finger print of the enhanced scattering cross-section of the carriers and reduced superconducting volume fraction [18].

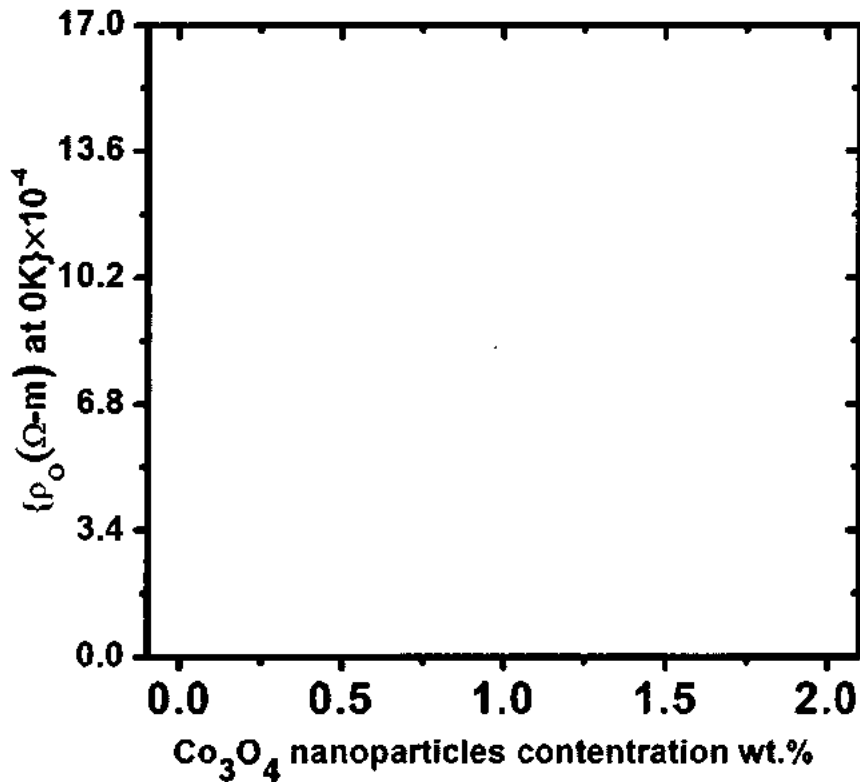


Fig. 4.7: The resistivity at normal state vs. nanoparticles concentration plot of $(\text{Co}_3\text{O}_4)_x/\text{CuTi-1223}$ nano-superconductor composites.

4.6 Activation energy

The information about flux pinning in superconductor is provided by activation energy (U). Activation energy (U) can be calculated by applying Arrhenius law. Activation energy provides information about the flux pinning strength in HTSCs. The Arrhenius plots of nanocomposite samples are shown in Fig. 4.8.

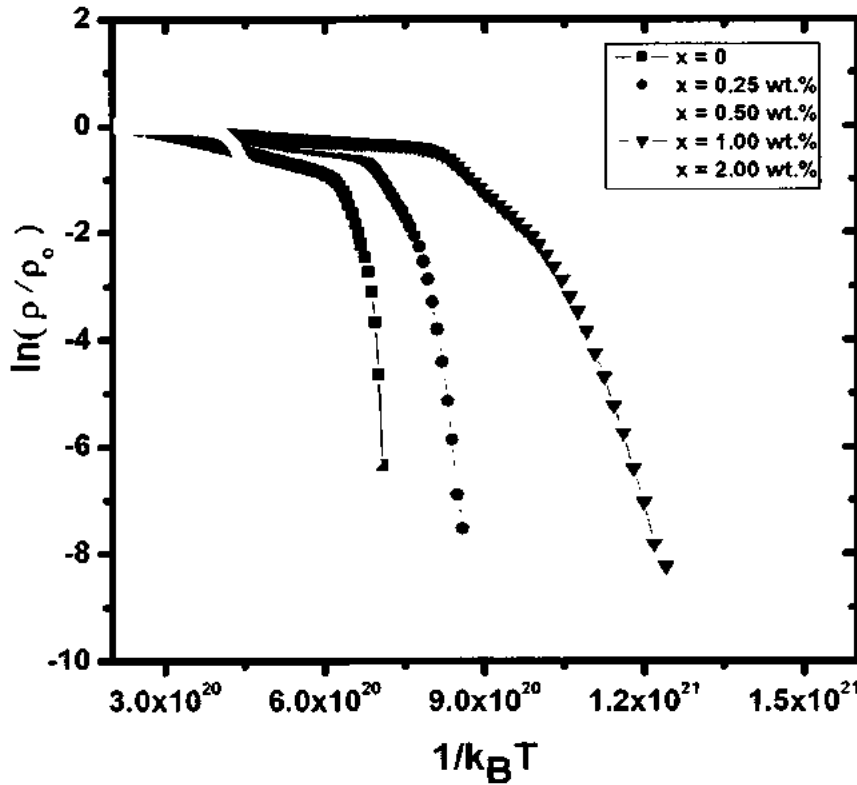


Fig. 4.8: Arrhenius plots of $(\text{Co}_3\text{O}_4)_x/\text{CuTi-1223}$ nano-superconductor composites with $x = 0, 0.25, 0.75, 1.0$ and 2.0 wt.%.

The Arrhenius law for superconductor can be written as;

$$\rho(T) = \rho_0 \exp(-U/k_B T) \dots\dots\dots(4.3)$$

where U represent activation energy and $k_B T$ is the thermal energy.

Taking “ln” on both sides of above equation we get;

$$\ln(\rho(T)) = \ln(\rho_0) - U/k_B T \dots\dots\dots(4.4)$$

We get a straight line by plotting this linear Eq (4.4) between the dependent quantity “ $\ln\rho(T)$ ” and the independent quantity “ $1/k_B T$ ”. The activation energy is indicated by U and we compare Eq. (4.4) with the intercept form of the straight line. I found the negative slope of this straight line i.e. $(-U)$ and y-intercept of that line “ $\ln(\rho_0)$ ”. In order to calculate to this energy it must be kept in mind that the region which is closer to T_c can be taken into account [19].

Fig. 4.9 demonstrates variation of activation energy and transition temperature T_c with concentration of nanoparticles. The activation energy decreases with increasing the concentration of nanoparticles in these superconducting composites [20].

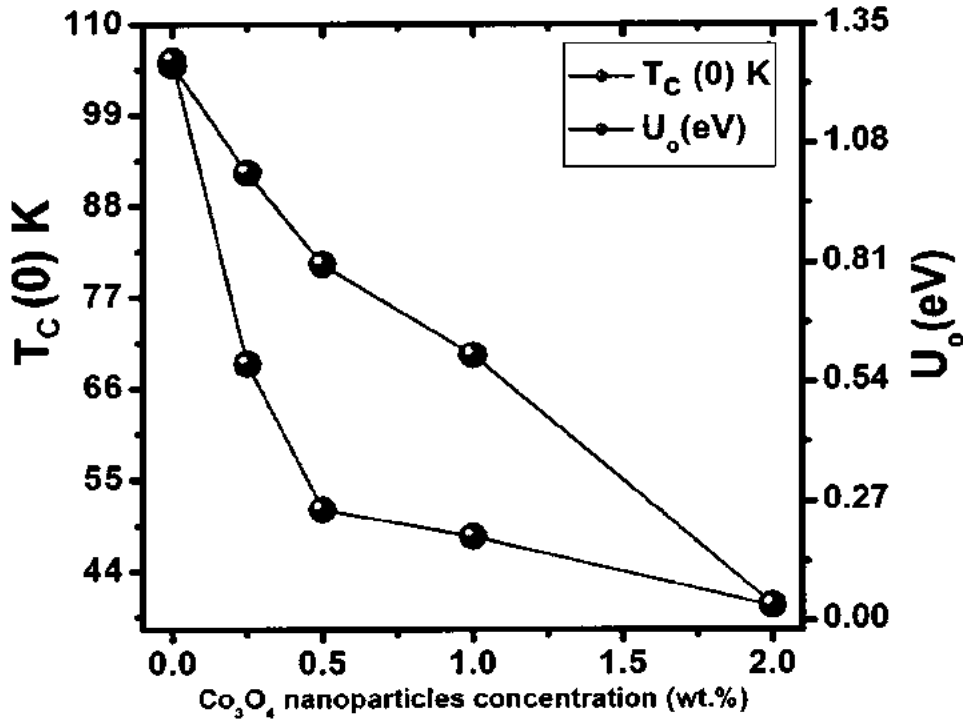


Fig. 4.9: Variation of T_c and activation energy with concentration of (Co_3O_4) nanoparticles in $(\text{Co}_3\text{O}_4)_x/\text{CuTi-1223}$ nano-superconductor composites with $x = 0, 0.25, 0.75, 1.0$ and 2.0 wt.%.

The activation energy is observed to decrease for the nanocomposites with $x = 0.25, 0.50, 1.0$ and 2.0 wt. % as compared to pure CuTi-1223 superconductor. Therefore flux pinning is decreased with increasing the concentration of nanoparticles in CuTi-1223 superconductor as compared to pure CuTi-1223 superconductor. The decrease in activation energy is attributed to agglomeration and inhomogeneous distribution of these antiferromagnetic nanoparticles at higher concentrations and scattering and breaking of Cooper pairs across the antiferromagnetic Co_3O_4 nanoparticles [21,22].

Conclusion

I successfully synthesized $(\text{Co}_3\text{O}_4)_x/\text{CuTl}$ -based nano-superconductor composites with $x = 0.0, 0.25, 0.50, 1.0$ and 2.0% by solid-state reaction method. XRD, FTIR spectroscopy and R-T measurements were used to study the structural properties and other parameters associated. We have found the average crystallite size of Co_3O_4 nanoparticles to be 71 nm which were synthesized by sol-gel method. It is concluded that the superconductor structure is not changed by adding the NPs having different concentrations as confirmed by the XRD results. Resistivity measurements reveal that the increase in the concentration of nanoparticles cause the smooth decrease in the critical temperature parameters of the superconductor such as $T_c(R = 0)$. Trapping of free carriers, scattering/localization of the charge carriers, and the reflection of spin charge are considered for this monotonic decrement. Resistivity at normal state also increases due to the scattering or localization of the carriers from antiferromagnetic Co_3O_4 nanoparticles. Weak flux pinning is the associated cause to the decrease of activation energy at high concentration of nanoparticles. In conclusion, superconducting properties of host CuTl-1223 matrix have been suppressed by the addition of antiferromagnetic Co_3O_4 nanoparticles.

References

1. M. Annabi, A. M. Chirgui, F. B. Azzouz, M. Zouaoui, and M. B. Salem, "Addition of Nanometer Al_2O_3 During the Final Processing of (Bi, Pb)-2223 Superconductors" *Physica C* **405**, 25-33 (2004).
2. J. B. Shi, Y. Hsu, and C. T. Lin, "Dielectric properties of Gd_2CuO_4 " *Physica C* **299**, 272–278 (1998).
3. F. T. J. Ngenefeme, N. J. Eko, Y. D. Mbom, N. D. Tantoh, and K. W. M. Rui, "A One Pot Green Synthesis and Characterization of Iron Oxide-Pectine Hybrid Nanocomposite" *J. Compos. Mater.* **3**, 30-37 (2013).
4. R. Zhangl, D. Gongl, X. Lu, S. Li, P. Dai, H. Luo, "The effect of Cr impurity to superconductivity to in electron-doped $\text{BaFe}_{2-x}\text{Ni}_x\text{As}_2$ " *Supercond. Sci. Technol.* **27**, 115003 (2014).
5. D. S. Sundaram, P. Puri, V. Yang, "Pyrophoricity of nascent and passivated aluminum particles at nano-scales, *Combust. Flame*" **160**, 1870–1875 (2013).
6. P. Puri, V. Yang, "Thermo-mechanical behavior of nano aluminum particles with oxide layers during melting" *J. Nanopart. Res.* **12**, 2989–3002 (2010).
7. M. Mumtaz, M. Kamran, K. Nadeem, A. Jabbar, Nawazish A. Khan, A. Saleem, S. T. Hussain, M. Kamran, "Dielectric properties of $(\text{CuO}, \text{CaO}_2, \text{ and BaO})_y/\text{CuTl-1223}$ composites" *Low Tem. Phys./Fiz. Nizk. Temp.* **39**, 806–814 (2013).
8. M. Mumtaz, Nawazish A. Khan, E. U. Khan, "Growth of $\text{Cu}_{0.5}\text{Tl}_{0.5}\text{Ba}_2\text{-Ca}_3\text{Cu}_4\text{-yZn}_y\text{O}_{12-\delta}$ superconductor with optimum carriers" *Physica C* **470**, 428–434 (2010).
9. A. Jabbar, I. Qasim, M. Waqee-ur-Rehamn, M. Zaman, K. Nadeem, and M. Mumtaz, "Structural and superconducting properties of $(\text{Al}_2\text{O}_3)_y/\text{CuTl-1223}$ composites" *J. Electron. Mater.* **44**, 110 (2015).
10. A. Jabbar, I. Qasim, K. M. Khan, Z. Ali, K. Nadeem, and M. Mumtaz "Synthesis and superconducting properties of $(\text{Au})_x/\text{CuTl-1223}$ composites" *J. Alloys Compd.* **618**, 110 (2015).
11. G. Bahmanrokh, M. Hashim, I. Ismail, N. Soltani, P. Vaziri, M. S. E. Shafie, M. Navaseri, "A simple method for measuring intrinsic blocking temperature in superparamagnetic nanomaterial", *J. Supercond. Nov. Magn.* **26**, 407–414 (2013).

12. M. Knobe, W. C. Nunes, H. Winnischofer, T. C. R. Rocha, L. M. Socolovsky, C. L. Mayorga, D. Zanchet, "Effects of magnetic inter-particle coupling on the blocking temperature of ferromagnetic nano-particle arrays", *J. Non-Cryst. Solids* **353**, 743–74 (2007).
13. R. V. Sarmago, K. L. C. Molina, L. J. D. Guerra, "A new perspective to AC magnetic susceptibility measurements in an unbalanced mutual inductance bridge", *Physica C* **364**, 239–242 (2001).
14. F. Gomory, "Characterization of high-temperature superconductors by AC susceptibility measurements", *Supercond. Sci. Technol.* **10**, 523–542 (1997).
15. K. Nadeem, G. Hussain, M. Mumtaz, A. Haider, S. Ahmed "Role of magnetic NiFe₂O₄ nanoparticles in CuTi-1223 superconductor" *Ceram. Int.* **41** 15041–15047 (2015).
16. Irfan Qasim, M. Waqeer-ur-Rehman, M. Mumtaz, K. Nadeem, "Role of Co nanoparticles in CuTi-1223 superconductors" *Ceram. Int.* **73**, 78 (2016).
17. K. Nadeem, F. Naeem, M. Mumtaz, S. Naeem, A. Jabbar, I. Qasim, Nawazish A. Khan, "Synthesis and characterization of core-shell Ni/NiO nanoparticles/CuTi-1223 superconductor composites", *Ceram. Int.* **40**, 13819–13825 (2014).
18. M. Waqee-ur-Rehman, I. Qasim, M. Mumtaz, K. Nadeem, S. Qamar, "Resistive transition and flux flow mechanism in CoFe₂O₄ nanoparticles added Cu_{0.5}Tl_{0.5}Ba₂Ca₃O_{10-δ} superconductor" *J. Alloys Compd.* **657**, 348 (2015).
19. R. Award, I. H. Ibrahim, E. M. E. Mansour, M. Roumie, "Magnetoresistance Studies of Tl-1223 Phase Substituted by Scandium" *J. Phys. Conf. Series*, **97**, 012323 (2008)
20. Waqee-ur-Rehman, M. Mumtaz, Irfan Qasim, K. Nadeem " Infield response of (Co)_x/CuTi-1223 nanoparticles- superconductor" *J. Cryogenics* **73**, 68-72 (2016).
21. M. Waqee-ur-Rehman, M. Mumtaz, Irfan Qasim, K. Nadeem " Infield superconducting properties of Ni nanoparticles added CuTi-1223 phase" *Solid state commun.* **228**, 32-35 (2016).
22. B. A. Albiss, I. M. Obaidat, M. Gharaibeh, H. Ghamlouche, and S. M. Obeidat, "Impact of addition of magnetic nanoparticles on vortex pinning and microstructure properties of Bi-Sr-Ca-Cu-O superconductor" *Solid State Commun.* **150**, 1542 (2010).